APPENDIX A
SPECIAL $\vec{k}$-POINT INTEGRAION

A.1. Introduction

Solid state calculations often involve integrations over the Brillouin zone (BZ) to obtain quantities such as the total energy, density of states, and optical response coefficients. Most of these integrations cannot be computed analytically because the integrands need to be evaluated numerically. The simplest method to approximate such integration is to evaluate the integrand at discrete $\vec{k}$-points and sum over these $\vec{k}$-points in the BZ. The computational time to carry out such calculations is proportional to the number of $\vec{k}$-points used. So it is important to choose as few $\vec{k}$-points as possible to produce the desired accuracy for such calculations. In 1973, Chadi and Cohen introduced a scheme to systematically generate the "special $\vec{k}$-points" for such purposes.[1] The number of $\vec{k}$-points generated by the Chadi-Cohen's scheme increases much too rapidly. To reach the next available $\vec{k}$-point set, one often needs to use nearly five times as many $\vec{k}$-points. In 1976, Monkhorst and Pack generalized the Chadi-Cohen's scheme to include all the Chadi-Cohen's $\vec{k}$-point sets and to add in the "missing" $\vec{k}$-point sets to bridge over from one Chadi-Cohen's set to another.[2] For the fcc lattice, the number of $\vec{k}$-points in the irreducible Brillouin zone (IBZ) increases as 1, $\underline{2}$, 6, $\underline{10}$, 20, 28, 46, $\underline{60}$, 84, 110, $\cdots$ in the Monkhorst-Pack's scheme. The Chadi-Cohen's $\vec{k}$-point sets are underlined and are a subset of the Monkhorst-Pack's $\vec{k}$-point sets.

Unlike the cubic structures, the $\vec{k}$-point sets for the hexagonal structure generated from the Chadi-Cohen's and the Monkhorst-Pack's schemes are different. This motived our study on the special $\vec{k}$-point generation. In this appendix, we show that the Monkhorst-Pack's scheme of generating $\vec{k}$-points can be further generalized. In the case of the hexagonal structure, the $\vec{k}$-point sets generated using this generalized scheme encompass all those by Chadi-Cohen and Monkhorst-Pack.[3] In addition, the generalized scheme produces more $\vec{k}$-point sets that are not included in either of the Chadi-Cohen's scheme or Monkhorst-Pack's scheme. Numerical convergence studies on the total-energy, the linear- and the nonlinear-optical responses plus the corresponding sum-rules show that the generalized $\vec{k}$-point sets work.

The main idea for generating the $\vec{k}$-points is the following. The quantities that are being integrated are periodic functions in the reciprocal lattice. The integrand can be formally expressed via Fourier transformation to a sum over its Fourier components. If the integration over the BZ is rigorous, only the zeroth Fourier component contributes; other Fourier components vanish upon integration. The $\vec{k}$-points should be chosen such that the sum over these $\vec{k}$-points should identically cancel out the low Fourier components. The lowest non-zero Fourier component that survives the sum over these $\vec{k}$-points gives an estimate of the error of such integration. Large $\vec{k}$-point sets can be generated to push this nonzero Fourier component to higher Fourier components at the cost of including more $\vec{k}$-points.

All $\vec{k}$-points of which we are aware lie on a lattice throughout the $\vec{k}$-space with unit weight associated with each lattice point. When all the $\vec{k}$-points are folded back into the IBZ using translational and rotational symmetries of the lattice, each point in the IBZ carries a different weight coming from the number of points folded onto that point. From this point of view, Monkhorst-Pack's scheme gives one way of constructing the $\vec{k}$-point lattices while the "generalized" scheme gives several topologically different ways of constructing the $\vec{k}$-point lattices. To minimize the number of the points after folding back into the IBZ, all the $\vec{k}$-point sets should obey the point group symmetry operations of the solid.

A.2. Theory

To briefly review the theoretical background of the special $\vec{k}$-point group integration, we will follow the approach of Chadi and Cohen.[1] Without loss of generality, we consider a function in $\vec{k}$-space $f(\vec{k})$ that is symmetric under all point symmetry operations of the lattice. To analyze the integration and summation of $f(\vec{k})$, we expand $f(\vec{k})$ in a symmetrized Fourier series with the coefficient of each Fourier component denoted by f_R,

$$f(\vec{k}) = f_0 + \sum_{R \neq 0} f_R A_R(\vec{k}) \tag{A.1}$$

in which $A_R(\vec{k})$ is the symmetrized Fourier component

$$A_R(\vec{k}) = \frac{1}{n_T} \sum_{|\vec{R}|=R} e^{i\vec{k}\cdot\vec{R}}. \tag{A.2}$$

The summation in Eq. (A.2) is over equivalent real space lattice vectors $\vec{R}$ related by lattice point group symmetry operations T_i^{-1}. There are n_T such symmetry operations. Integration of $f(\vec{k})$ over the BZ gives

$$\frac{\Omega_0}{(2\pi)^3}\int_{BZ} d\vec{k} f(\vec{k}) = n_T \frac{\Omega_0}{(2\pi)^3}\int_{IBZ} d\vec{k} f(\vec{k}) = f_0, \tag{A.3}$$

in which Ω_0 is the unit cell volume. If we choose a set of special $\vec{k}$-points weighted by w_i which for some R_1 corresponds to

$$S(R) = \sum_{i=1}^{n} w_i A_R(\vec{k}_i) = 0, \quad \text{for } R < R_1, \tag{A.4}$$

the summation of $f(\vec{k})$ over the these special $\vec{k}$-points gives a good approximation to the integration. Denoting those R which make $S(R) \neq 0$ by $R_1 < R_2 < \cdots$, we can write the sum of $f(\vec{k})$ over these $\vec{k}$-points by

$$\sum_{i=1}^{n} w_i f(\vec{k}_i) = f_0 + f_{R_1} S(R_1) + f_{R_2} S(R_2) + \cdots, \tag{A.5}$$

where the leading error of approximating the integration with summation can be approximated by $f_{R_1} S(R_1)$.*

In the search for special $\vec{k}$-points in 2-dimensional hexagonal lattice, we have found a systematic way of generating them. With our new method, we not only recover all the special $\vec{k}$-point sets by Chadi and Cohen,[1] Monkhorst and Pack,[2] but also provide new ones. We characterize the special $\vec{k}$-point sets we generated into four different groups. An example of each group is shown in Figure A.1. Group I is identical to Monkhorst and Pack's sets.[2,3] The special $\vec{k}$-point sets by Chadi and Cohen[1] turn out to be a few of the elements of Groups II and IV. Sets in Group III are new. Figure A.1 shows that the difference between the special $\vec{k}$-points in

* If $f(\vec{k})$ is infinitely differentiable in addition to being periodic, then $f_{R\to\infty}$ approaches zero faster[4] than any inverse power of R.

Groups I and III (II and IV) is a 30° rotation in the orientation of the special $\vec{k}$-points. However, as we will show in the next section, the orientation of the special $\vec{k}$-points can affect the accuracy of the integration.

For each special $\vec{k}$-point set in Group I (III), there exists a corresponding set in Group II (IV) with the same R_i to make $S(R_i) \neq 0$. However, sets in Groups I (III) and II (IV) have different values for $S(R_i)$:

$$\sum_{\vec{k}_i \in I(III)} w_i f(\vec{k}_i) = f_0 + n_T f_{R_1} + n_T f_{\sqrt{3}R_1} + \cdots, \tag{A.6a}$$

$$\sum_{\vec{k}_i \in II(IV)} w_i f(\vec{k}_i) = f_0 - \frac{1}{2} n_T f_{R_1} + n_T f_{\sqrt{3}R_1} + \cdots. \tag{A.6b}$$

It can be shown that $R_2 = \sqrt{3}R_1$ for all sets in all four groups. We note here that R_1 of Groups III and IV differ from those of Groups I and II. To see this difference consider $\vec{R}_1$ and $\vec{R}_2$ for different groups. We chose the basis vectors, $\hat{a}$ and $\hat{b}$, for the crystal coordinates to be related to the Cartesian coordinates basis vectors, $\hat{x}$ and $\hat{y}$, by $\hat{a} = \hat{x}$, $\hat{b} = -\hat{x}/2 + \sqrt{3}\hat{y}/2$. The $\vec{R}_1$ and $\vec{R}_2$ for the four different groups are

$$\begin{aligned} \vec{R}_1^{(I,II)} &= T_i(n\hat{a}), & \vec{R}_2^{(I,II)} &= T_i(2n\hat{a} + n\hat{b}), \\ \vec{R}_1^{(III,IV)} &= T_i(2m\hat{a} + m\hat{b}), & \vec{R}_2^{(III,IV)} &= T_i(3m\hat{a}), \end{aligned} \tag{A.7}$$

where $T_i\vec{R}$ are related to $\vec{R}$ by the symmetry operations T_i.

It follows directly from Eq. (A.6) that special $\vec{k}$-point integrations involving the two corresponding sets in Groups I and II (III and IV) can be used to cancel the leading errors by a weighted average of the two results, namely

$$\begin{aligned} &\frac{1}{3} \sum_{\vec{k}_i \in I(III)} w_i f(\vec{k}_i) + \frac{2}{3} \sum_{\vec{k}_j \in II(IV)} w_j f(\vec{k}_j) \\ =&f_0 + 0 + n_T f_{\sqrt{3}R_1} + \cdots = \sum_{\vec{k}_l \in III(I)} w_l f(\vec{k}_l). \end{aligned} \tag{A.8}$$

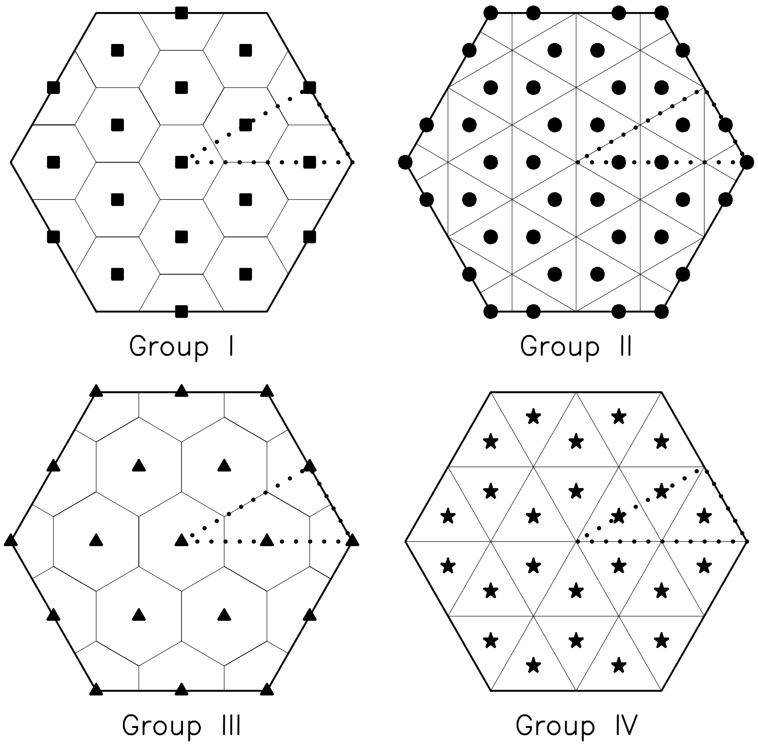

FIGURE A.1 Special $\vec{k}$-points in the Brillouin zone belonging to four different groups in two-dimensional hexagonal lattice. In Groups I and III, the special $\vec{k}$-points are at the centers of hexagons, while in Groups II and IV, they are at the centers of triangles. The hexagons (triangles) in Group III (IV) are rotated 30° from the orientation of the hexagons (triangles) in Group I (II). The corners of the Group I hexagons (Group II triangles) are the positions of the special $\vec{k}$ points in Group II (I). Groups III and IV are similarly related. These figures show the cases for which the number of special $\vec{k}$ points in the irreducible zone (indicated by dotted lines) are 4, 5, 4, and 3 for Groups I, II, III, and IV, respectively (see Table A.2). By varying the size of the hexagons or triangles, we can obtain other point sets in the different groups. Adding the $\vec{k}$-points with the same R_1 [cf. Eq. (A.5)] in Groups I and II (or III and IV), such as the sets in this figure, yields another set in Group III (I).

This is an example of Richardson extrapolation.[5] Two numerical example demonstrating Eq. (A.8) will be presented in the next section.

A.3. Numerical Study

To demonstrate of the effectiveness of Eq. (A.8) for the special $\vec{k}$-point integration, we give two numerical examples in Table A.1. In column 3 of both cases, the results in row 3 (7) obtained by Richardson extrapolation are very close to the results in row 4 (8) that are direct LDA calculations using the combined special $\vec{k}$-points. The close agreement between the two methods enabled us to use Eq. (A.8) to extrapolate some results instead of doing another calculation in the numerical studies shown in Figures A.2 and A.3.

In the convergence study of the LDA total ground state energy (Figure A.2), we observe that in the range of R_1 up to $R_1 = 7$, E_{tot} from the special $\vec{k}$-point sets in Groups III and IV are much closer to the converged value than those of Groups I and II for reasons not yet understood. This fact appears to conflict with the general belief[1,2] that the convergence of the special $\vec{k}$-point integration should depend most heavily on the *magnitude* of $\vec{R}_1$ and with only slight dependence on its *direction*. Figure A.2 verifies that, in the same Group, the error decreases with increasing R_1. On the other hand Figure A.2 also shows that in the same R_1 range, there can be an order of magnitude difference if $\vec{R}_1$ is pointing at a different direction. [$\vec{R}_1^{(I,II)} = T_i(n\hat{a})$, $\vec{R}_1^{(III,IV)} = T_i(2m\hat{a} + m\hat{b})$ in the crystal coordinates.]

The optical response calculations are more time consuming than LDA ground state runs, so we do not have as complete a convergence study on the optical

TABLE A.1 Numerical demonstration of the extrapolation formula of Eq. (A.8) for the four special $\vec{k}$-point sets shown in Figure A.1. The top half of the table demonstrates (Group I + 2×Group II)/3 = Group III; the bottom half (Group III + 2×Group IV)/3 = Group I. The values shown are the difference between the LDA total energies calculated with different $\vec{k}$-point sets E_{tot} and the converged value $E^*_{tot} = -131988.30$ meV taken from Figure A.2 at $R \approx 26$. The extrapolated results given in row 3 (7) closely agree with row 4 (8); the difference is due to the fact that slightly different self-consistent potentials (for different number of special $\vec{k}$-points) are used. This close agreement enables us to predict the results represented by open symbols in Figures A.2 and A.3. Data shown in this table can also be found in Figure A.2. Calculations shown in this table and in Figures A.2 and A.3 are all done on 2H-SiC (wurtzite) with E_{cut}=17 hartree and 2 layers of special $\vec{k}$-points in the z-direction of the irreducible Brillouin zone.

No. of $\vec{k}$-points in IBZ per layer (Group, R_1)	Method	$E_{tot} - E^*_{tot}$ (meV/atom)
4(I, 4)	LDA	−33.76
5(II, 4)	LDA	16.37
[4(I,4) + 2×5(II,4)]/3	Richardson[5]	−0.34
9(III, $4\sqrt{3}$)	LDA	−0.23
4(III, $2\sqrt{3}$)	LDA	−3.34
3(IV, $2\sqrt{3}$)	LDA	−2.36
[4(III,$2\sqrt{3}$) + 2×3(IV,$2\sqrt{3}$)]/3	Richardson[5]	−2.68
7(I, 6)	LDA	−2.70

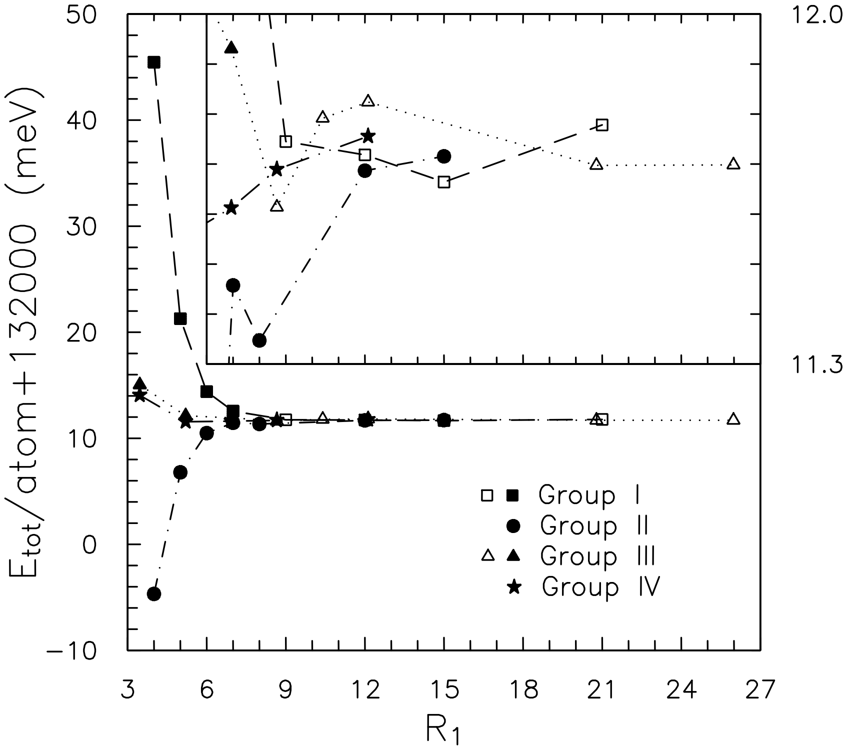

FIGURE A.2 Convergence of the LDA total energy as a function of R_1 – radius of the first ring when $S(R)$ [see Eq. (A.5)] is nonzero – for four groups of the special $\vec{k}$-points shown in Figure A.1. The E_{tot}/atom obtained by the special $\vec{k}$-point sets from all four groups converge to approximately the same value as R_1 increases. For comparable R_1, results from Groups III and IV are much closer to the converged value than results from Groups I and II for reasons not yet understood. The original calculations (solid symbols) can be extended by combining two results [see Eq. (A.8)] to yield a result at a larger R_1 (open symbol) (e.g., and at R_1=6 combine to yield $\triangle$ at $R_1 = 6\sqrt{3} \approx 10.4$). Insert shows the details for $R_1 > 6$.

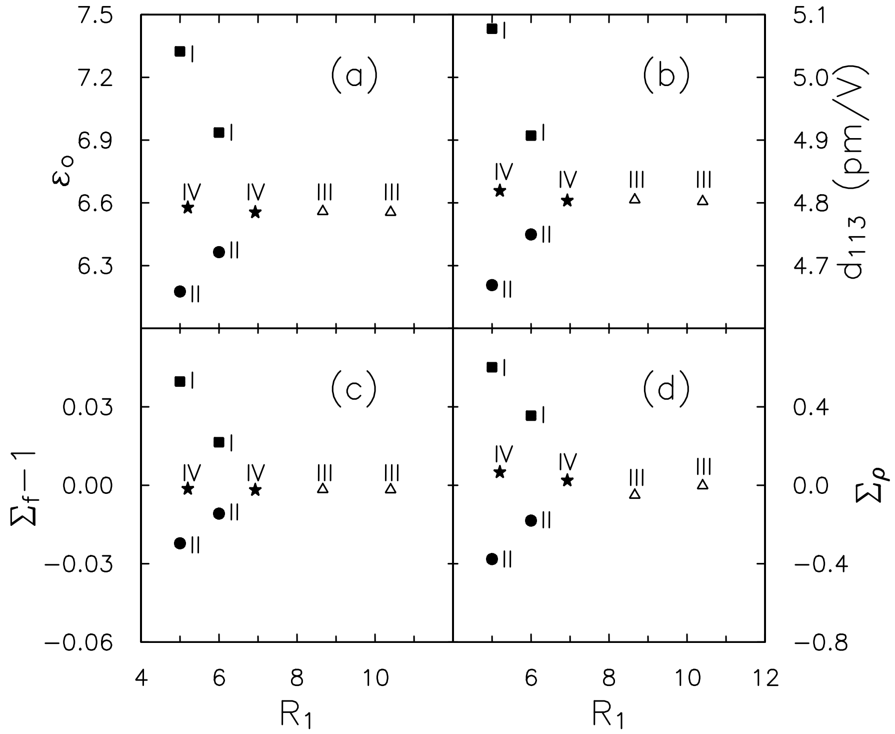

FIGURE A.3 Convergence study on 2H-SiC of the dielectric constant ε_o and the second-harmonic generation coefficient d_{xxz} and of the associated sum rules Σ_f [Eq. (2.38) of Ref. 6] and Σ_ρ [Eq. (13) of Ref. 7] as a function of R_1 for four groups of special $\vec{k}$-points. For similar R_1, the results from Group IV are much closer to the converged values than Groups I and II, same as in Figure A.2. In each panel, the points in Group III at R_1=8.66 and 10.39 are obtained by averaging the two values of Groups I and II at R_1=5 and 6 with twice the weight given to the result from Group II [see Eq. (A.8)]. The sum rule Σ_f has an ideal value of 1, and Σ_ρ has a possible range of [−2, 2] and an ideal value of 0.

response as on the LDA ground state total energy. However, the existing data on the convergence properties of the optical response have the same facts (1) and (2) as those of the LDA E_{tot} [see Figure A.3]. This indicates that the special $\vec{k}$-point sets in Groups III and IV are the preferred sets for integration at least for the wurtzite structure. Between Groups III and IV, sets in Group III have fewer special $\vec{k}$-points in the irreducible Brillouin zone for $R_1 \geq 5\sqrt{3} \approx 8.66$. So sets in Group III are preferred in the range $R_1 \geq 8.66$ and sets in Group IV are preferred in the range $R_1 < 8.66$. We present the special $\vec{k}$-point numbers for four different groups for 2-dimensional hexagonal lattice in Table A.2.

A.4. Discussion

We have demonstrated using the generalized scheme to generate the special $\vec{k}$-point sets for the hexagonal lattice. In this section, we will briefly discuss how to apply the generalized scheme to the cubic lattices.

We begin with the one dimensional (1-D) case. There are two groups of special $\vec{k}$-points for 1-D BZ integration: (1) Group I includes the Γ point; (2) Group II is a shift of the $\vec{k}$-points in Group I to exclude the Γ point. As shown in Figure A.4, the corresponding set in Group II is preferred because it has fewer points in the IBZ. Combining Groups I and II using the Richardson extrapolation scheme as explained in Sec. A.2, yields another set in Group I and does not produce any new groups of $\vec{k}$-points. However, as we will discuss next for 2-D and 3-D, Richardson extrapolation gives new $\vec{k}$-point sets that do not belong in the old groups.

In the 2-D square lattice, the $\vec{k}$-point sets in Group I (II) can be obtained by repeating the 1-D $\vec{k}$-point sets in Group I (II) in both $\hat{x}$ and $\hat{y}$ directions. As shown

TABLE A.2 Number of special $\vec{k}$-points in the irreducible Brillouin zone versus R_1 for different special $\vec{k}$-point groups in the 2-dimensional hexagonal lattice. General expressions for the number of $\vec{k}$-points listed at the bottom of the table only exist for some $\vec{k}$-point sets.

R_1	Group I	Group II	Group III	Group IV
1	1	1		
$\sqrt{3}$			2	1
2	2	2		
3	3	3		
$2\sqrt{3}$			4	3
4	4	5		
5	5	7		
$3\sqrt{3}$			6	6
6	7	9		
$4\sqrt{3}$			9	10
7	8	12		
8	10	15		
$5\sqrt{3}$			12	15
9	12	18		
10	14	22		
$6\sqrt{3}$			16	21
$2n\sqrt{3}$			n^2+2n+1	$2n^2+n$
$(2n+1)\sqrt{3}$			n^2+3n+2	$2n^2+3n+1$
$6n$	$3n^2+3n+1$	$6n^2+3n$		
$6n+3$	$3n^2+6n+3$	$6n^2+9n+3$		

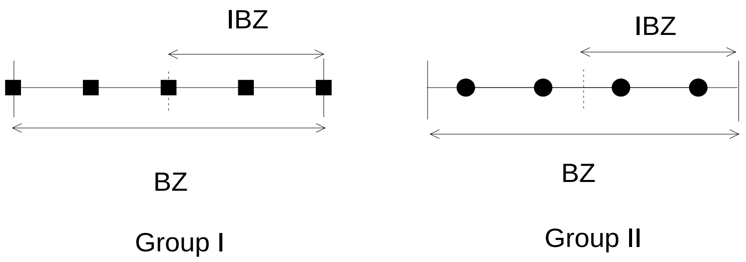

FIGURE A.4 Special $\vec{k}$-points for the 1-D Brillouin zone. The special $\vec{k}$-point sets in Group I contain the Γ point; the ones in Group II do not. The $\vec{k}$-point sets in Group II are preferred because the corresponding set [i.e., with the same R_1 in Eq. (A.5)] in Group II has fewer points in the IBZ. The Monkhorst-Pack's $\vec{k}$-point sets for cubic structures in 2-D (3-D) can be obtained by repeating the 1-D $\vec{k}$-points in 2 (3) directions.

in Figure A.5, the corresponding set in Group II has fewer points in the IBZ hence is preferred. Combining the two sets in Groups I and II in Figure A.5 gives the set in Group III. A rigid shift of the points in Group III to exclude the Γ points yields the set Group IV. Combining the two sets in Groups III and IV gets back at Group I. Groups IV is preferred over Group III because its corresponding sets contain fewer points in the IBZ. Between Groups II and IV, however, one cannot determine which is more efficient without numerical evidence or knowledge of the $\vec{k}$-dependence of the quantity being integrated. The $\vec{k}$-point sets for the 2-D square lattice can be applied to cubic lattices with strain in the (0,0,1) and equivalent directions. Groups I and II for the square are generated by the Monkhorst-Pack's scheme[2] but Groups III and IV are new.

More interesting is the 3-D case. Just as in 2-D, the Monkhorst-Pack's $\vec{k}$-point sets in 3-D can be generated by repeating the 1-D $\vec{k}$-points in all $\hat{x}$, $\hat{y}$, and $\hat{z}$

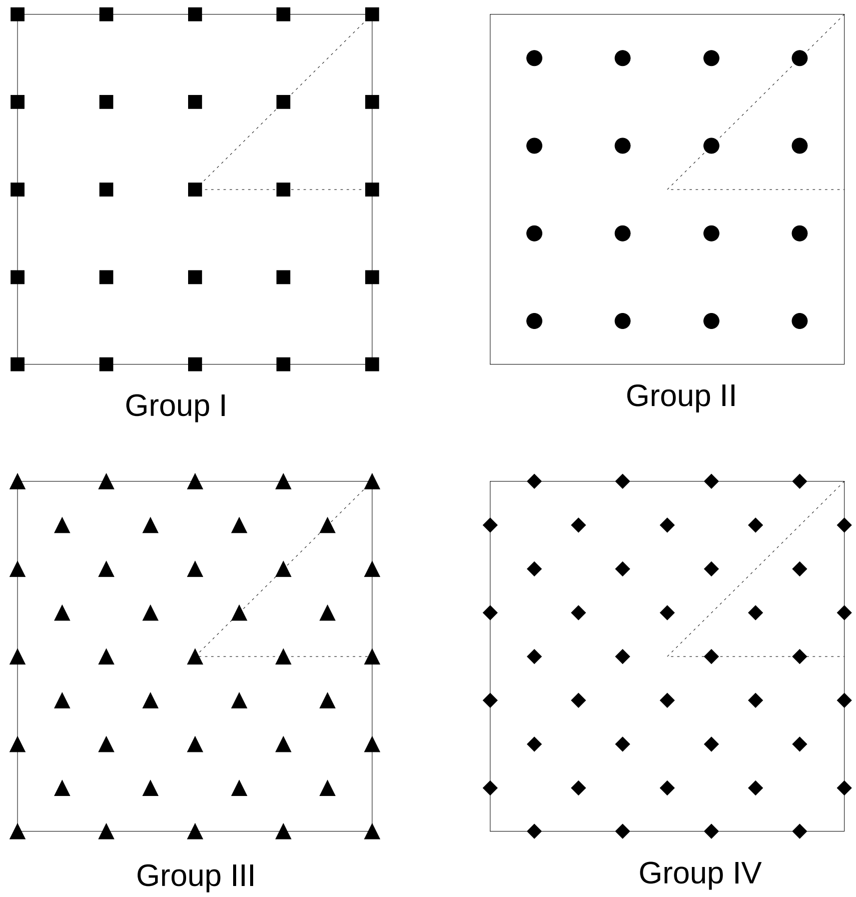

FIGURE A.5 Special $\vec{k}$-points for the 2-D square lattice. The $\vec{k}$-points in Groups I and II form a square lattice and can be generated by the Monkhorst-Pack's scheme. The $\vec{k}$-point set in Group III can be obtained by superimposing the corresponding sets in Groups I and II. Group IV is a rigid shift of the $\vec{k}$-points in Group III to exclude the Γ point. The $\vec{k}$-points in Group III (IV) also form a square lattice which is a 45° rotation from the $\vec{k}$-points in Group I (II). Combining the points in Groups III and IV yields another $\vec{k}$-point set in Group I.

directions. The points generated using the Monkhorst-Pack's scheme form a simple cubic lattice. Using the generalized scheme, the fcc or bcc lattice of $\vec{k}$-points are also valid choices. Applying Richardson extrapolation produces more groups of $\vec{k}$-points none of which have been explored.

All discussions so far have been confined to the case where the $\vec{k}$-points in the extended $\vec{k}$-space form a lattice with each $\vec{k}$-point carrying the same weight. One can make further generalization to have $\vec{k}$-points form lattices with a basis (e.g., the diamond structure) and put different weights on different points. When exploring different possibilities of generating $\vec{k}$-points, Eq. (A.2) should be used as a guideline to estimate the effectiveness of the $\vec{k}$-points.

APPENDIX B
CALCULATION OF SPIN-ORBIT COUPLING USING PSEUDOPOTNTIALS

B.1. Introduction

Spin-orbit coupling is one of three first-order relativistic corrections coming from the Dirac equation. The other two – the Darwin term and the mass-velocity term – combine to give the "scalar-relativistic" corrections which are included in standard pseudopotentials.[8] The problem of calculating the spin-orbit coupling using the pseudopotential method, however, is not fully solved. The spin-orbit coupling is important for heavy elements. From Si to Ge to InSb, the spin-orbit splitting at Γ point of the top of the valence band grows from 0.04 eV to 0.29 eV to 0.9 eV, while the band gap at Γ point decreases from 2.5 eV to 0.9 eV to 0.2 eV. When the spin-orbit splitting becomes comparable to the band gap, it has a significant effect on various physical properties including the effective mass, and the optical response.

There are two proposed methods to construct pseudopotentials for spin-orbit coupling. Method one[9] uses "semi-local" pseudopotentials that requires evaluation of a large number of integrals proportional to the square of the number of plane-waves used, which can become a bottleneck of these calculations. This problem associated with method one was solved by method two[10] using "fully-separable" (Kleinman-Bylander type[11]) pseudopotentials. However, the expressions of the pseudopotentials of method two are long and difficult to derive.

We propose a new method of constructing the "fully-separable" pseudopotentials that is shorter and easier to derive. The final form of our pseudopotentials is also physically transparent. Our calculated spin-orbit splittings of semiconductors are in good agreement with experiment and with the values obtained using other methods.

The spin-orbit Hamiltonian for an electron in a self-consistent potential $V(\vec{r})$ takes the form

$$\begin{aligned} H_{so} &= \frac{1}{2m^2c^2}\vec{S}\cdot\left[\vec{P}\times\vec{\nabla}V(\vec{r})\right] \\ &\approx -\frac{1}{2m^2c^2}\frac{1}{r}\frac{dV(r)}{dr}\vec{L}\cdot\vec{S}. \qquad \longleftarrow \text{Spherical approximation} \end{aligned} \tag{B.1}$$

To date, this spherical approximation is made for all solid state calculations we are aware of. The error of the spherical approximation is small because most of the relativistic effects come from the core region with a deep potential hence large velocity of the electrons. Figure B.1 shows that over 99% of the spin-orbit effect for the atomic Ge 4p electrons comes from inside the radius of 0.5 bohr which is much smaller than half the atomic distance of 2.3 bohr in solid Ge. Inside the core region, the potential in the solid is mostly spherical and atomic like. So the spherical approximation is justified. In calculations such as those using linear-muffin-tin orbitals or linear-augmented plane-waves methods,[12] the potential in the solid is known not only in the bonding region but also in the core region. In those all

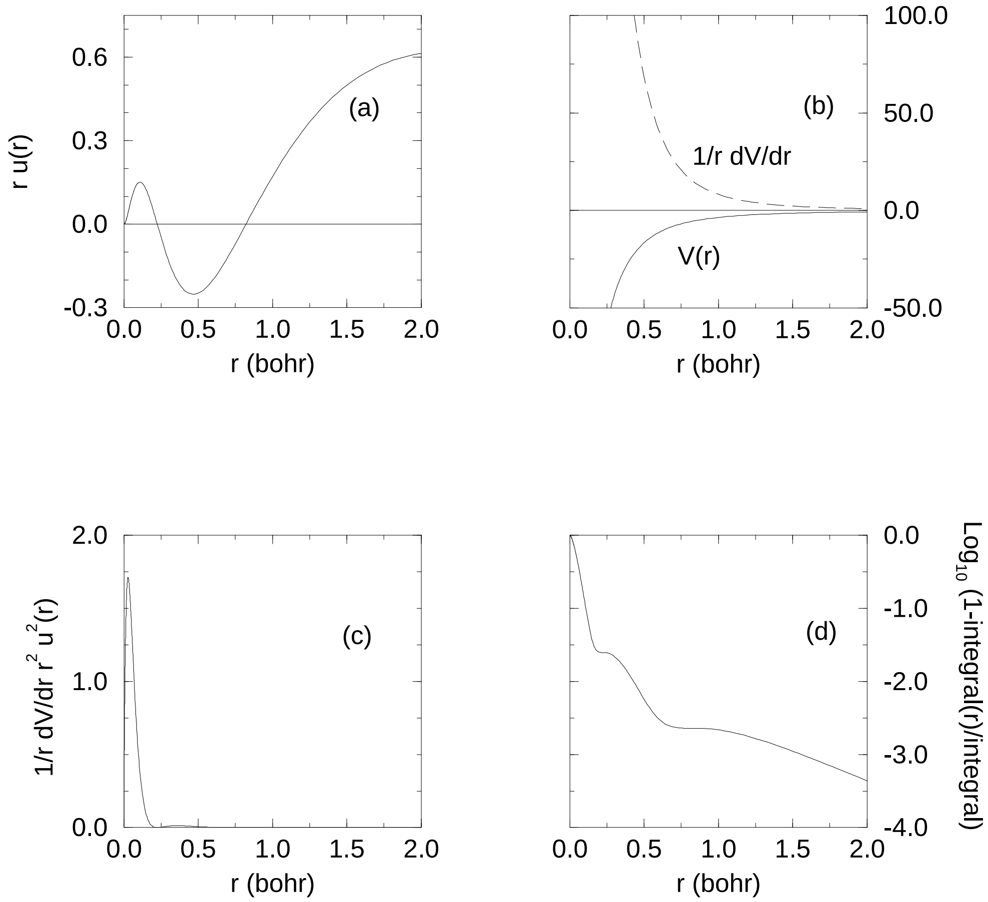

FIGURE B.1 Calculations on Ge atom. Figure (a) shows the radial wavefunction $ru(r)$ for the $4p$ electrons in which $\psi(\vec{r}) = u(r)Y_{lm}(\hat{r})$. Figure (b) shows the self-consistent atomic potential $V(r)$ and $1/r(dV/dr)$, both of which diverge at the origin. Figure (c) shows that the integrand $1/r(dV/dr)r^2u^2(r)$ is strongly peaked very close to the origin. There is little contribution beyond 0.5 bohr. This is also illustrated in Figure (d) which plots $\log_{10}\{1 - \int_0^r dr[1/r(dV/dr)r^2u^2(r)]/\int_0^\infty dr[1/r(dV/dr)r^2u^2(r)]\}$. Figure (d) shows that over 99% of the contribution to the spin-orbit splitting comes from $r < 0.5$ bohr. In the solid, the potential change inside the core region is very small compared to the atomic potentials, which justifies the spherical approximation and the atomic potential approximation discussed in the text.

electron methods, the spin-orbit coupling Hamiltonian can be obtained by taking the radial derivative of $V(r)$ inside the muffin-tin radius and using Eq. (B.1).[12] For calculations using pseudopotentials, however, the real physical potential in the core region is replaced by a soft pseudized potential. The spin-orbit Hamiltonian is not related to the derivative of this pseudized potential. To obtain the spin-orbit Hamiltonian for the pseudopotential calculations, one needs to approximate the potential in the core region by the atomic potential. For $r < r_c$, a core radius,

$$V_{solid}(r < r_c) \approx V_{atom}(r < r_c), \qquad \longleftarrow \text{Atomic potential approximation.} \tag{B.2}$$

Since the solid potential in the core is changed little from the atomic one, Eq. (B.2) is as good an approximation as the spherical approximation. Another way of understanding the atomic potential approximation is that the difference between the spin-orbit splitting in the solid and in the atom comes almost entirely from the difference in the distribution of the valence charge. As will be shown in Sec. B.3, the close agreement between our calculated values of spin-orbit splittings and the experimental ones indicate that the two approximations – the spherical approximation and the atomic potential approximation – give very little error.

B.2. Theory

To construct pseudopotentials, we first solve the Dirac equation in an atom with local-density approximation. The normalized major components of the wave functions are pseudized* to get the pseudo wavefunctions $u_{j=\ell\pm 1/2}(r)$; j and ℓ are

* We follow Troullier-Martins' suggestion[13] to match the value plus four derivatives of the pseudo-wavefunction and the atomic wavefunction at the matching radius. The weight of the pseudo-wavefunction inside the matching radius is equal to that of the atomic wavefunction.

total angular momentum and orbital angular momentum, respectively. Inverting the Schrödinger equation on $u_{j=\ell\pm 1/2}(r)$ yields the corresponding pseudopotentials $V_{\ell\pm 1/2}(r)$. We take the degeneracy weighted average of the $\ell = 3$ potentials as the local potential $V^{LOC}(r) = [3V_{5/2}(r) + 4V_{7/2}(r)]/7$ and denote the rest by

$$v_{\ell\pm 1/2}(r) = V_{\ell\pm 1/2}(r) - V^{LOC}(r), \qquad \ell = 1, 2. \tag{B.3}$$

(Of course, the s potential does not split.) All $V_{\ell\pm 1/2}(r)$ are, by construction,[13] identical beyond the matching radius; thus, via Eq. (B.3), $v_{\ell\pm 1/2}(r)$ are short range. We can write the nonlocal piece of the pseudopotential directly in the Kleinman-Bylander form[11] with the projection operators being $|\ell, j, m_j\rangle$,

$$\begin{aligned} V^{NL} =& \sum_{\ell}\sum_{m_j} |\ell, j = \ell + 1/2, m_j\rangle |V_\ell^{+}\rangle\langle V_\ell^{+}| \langle \ell, j = \ell + 1/2, m_j| \\ &+ \sum_{\ell}\sum_{m_j} |\ell, j = \ell - 1/2, m_j\rangle |V_\ell^{-}\rangle\langle V_\ell^{-}| \langle \ell, j = \ell - 1/2, m_j|, \end{aligned} \tag{B.4}$$

where the projection operators are

$$|V_\ell^{\pm}\rangle \equiv |v_{\ell\pm 1/2} u_{\ell\pm 1/2}\rangle / \langle u_{\ell\pm 1/2}| v_{\ell\pm 1/2} | u_{\ell\pm 1/2}\rangle^{1/2}. \tag{B.5}$$

We need a pseudopotential which has local $V^{LOC}(r)$ and nonlocal V^{NL} pieces with the nonlocal piece written in the Kleinman-Bylander form[11] containing the ionic v_ℓ^{ion} and the spin-orbit v_ℓ^{so} contributions. Specifically, we demand

$$\begin{aligned} V =& V^{LOC}(r) + V^{NL} \\ =& V^{LOC}(r) + \sum_{s_z=\pm 1/2}\sum_{\ell}\sum_{m=-\ell}^{\ell} |\ell, m, s_z\rangle V_\ell^{NL} \langle \ell, m, s_z|, \end{aligned} \tag{B.6}$$

where

$$V_\ell^{NL} = v_\ell^{ion} + v_\ell^{so} \vec{L}\cdot\vec{S}.$$

Rewriting Eq. (B.6) in the basis $|\ell, j, m_j\rangle$ gives

$$
\begin{aligned}
V^{NL} &= \sum_{\ell} \sum_{j} \sum_{m_j} |\ell, j, m_j\rangle \left[v_\ell^{ion} + v_\ell^{so} \vec{L} \cdot \vec{S} \right] \langle \ell, j, m_j| \\
&= \sum_{\ell} \sum_{m_j} |\ell, j = \ell + 1/2, m_j\rangle \left[v_\ell^{ion} + \frac{\ell}{2} v_\ell^{so} \right] \langle \ell, j = \ell + 1/2, m_j| \\
&\quad + \sum_{\ell} \sum_{m_j} |\ell, j = \ell - 1/2, m_j\rangle \left[v_\ell^{ion} - \frac{\ell + 1}{2} v_\ell^{so} \right] \langle \ell, j = \ell - 1/2, m_j|.
\end{aligned}
\tag{B.7}
$$

The second equal sign holds because $|\ell, j = \ell \pm 1/2, m_j\rangle$ are eigenstates of $\vec{L} \cdot \vec{S}$. Comparison of Eqs. (B.4) and (B.7) yields

$$
\begin{cases}
v_\ell^{ion} = \frac{\ell + 1}{2\ell + 1} |V_\ell^+\rangle\langle V_\ell^+| + \frac{\ell}{2\ell + 1} |V_\ell^-\rangle\langle V_\ell^-| \\
v_\ell^{so} = \frac{2}{2\ell + 1} |V_\ell^+\rangle\langle V_\ell^+| - \frac{2}{2\ell + 1} |V_\ell^-\rangle\langle V_\ell^-|.
\end{cases}
\tag{B.8}
$$

Eq. (B.8) is very similar to the form proposed by Hybertsen and Louie for the semilocal pseudopotentials.[9] The only difference between the Hybertsen-Louie method and ours is that in the former, the semilocal potentials were used to give weighted average/difference for the ionic/spin-orbit pseudopotentials whereas in the latter case, the Kleinman-Bylander potentials, i.e., the projection operators, are used.

In the solid calculation, the spin-orbit Hamiltonian is treated as a perturbation in our current implementation. We first solve the non-spin-orbit LDA Hamiltonian H_0 to obtain the eigenvalues $\epsilon_{n\vec{k}}$ and the corresponding eigenstates

$$
\langle \vec{r} | n\vec{k} \rangle = \sum_{\vec{G}} c_{n\vec{k}}(\vec{G}) e^{i\vec{G}\cdot\vec{r}} \qquad \text{(no splitting)}, \tag{B.9}
$$

in which n is the band index and $\vec{G}$ is the reciprocal lattice vector. Second we compute the matrix element of the spin-orbit Hamiltonian $H_{so} = v_{so}\vec{L} \cdot \vec{S}$ between the non-split eigenstates

$$
\begin{aligned}
&\langle n_1\vec{k}\uparrow|H_{so}|n_2\vec{k}\uparrow\rangle = -\langle n_1\vec{k}\downarrow|H_{so}|n_2\vec{k}\downarrow\rangle \\
=&\sum_{\pm}\sum_{\alpha}\sum_{\ell}\sum_{m=-\ell}^{\ell}\pm\frac{m}{2\ell+1}G_{\pm}(\alpha,n_1,\ell,m)G^{*}_{\pm}(\alpha,n_2,\ell,m) \\
&\langle n_1\vec{k}\uparrow|H_{so}|n_2\vec{k}\downarrow\rangle = \langle n_1\vec{k}\downarrow|H_{so}|n_2\vec{k}\downarrow\rangle^{*} \\
=&\sum_{\pm}\sum_{\alpha}\sum_{\ell}\sum_{m=-\ell}^{\ell}\pm\frac{\sqrt{(\ell+m+1)(\ell-m)}}{2\ell+1}G_{\pm}(\alpha,n_1,\ell,m)G^{*}_{\pm}(\alpha,n_2,\ell,m)
\end{aligned}
\tag{B.10}
$$

in which

$$
\begin{aligned}
G_{\pm}(\alpha,n,\ell,m) =&4\pi\sum_{\vec{G}}c_{n\vec{k}}(\vec{G})Y_{\ell m}(\vec{k}+\vec{G})e^{-i\vec{G}\cdot\tau_{\alpha}} \\
&\times\frac{2}{2\ell+1}\int_{0}^{\infty}j_{\ell}(|\vec{k}+\vec{G}|r)V^{\pm}_{\ell}(r)r^{2}dr,
\end{aligned}
\tag{B.11}
$$

and where τ_α is the lattice coordination of atomic type α in the unit cell and $j_\ell(x)$ are the spherical Bessel functions. Next we add the spin-orbit Hamiltonian matrix to the non-spin-orbit one to obtain the full Hamiltonian matrix

$$
\begin{aligned}
\langle n_1\vec{k}\sigma_z|H|n_2\vec{k}\sigma'_z\rangle =&\langle n_1\vec{k}\sigma_z|H_0|n_2\vec{k}\sigma'_z\rangle + \langle n_1\vec{k}\sigma_z|H_{so}|n_2\vec{k}\sigma'_z\rangle \\
=&\epsilon_{n_1\vec{k}}\delta_{n1,n2}\delta_{\sigma_z,\sigma'_z} + \langle n_1\vec{k}\sigma_z|H_{so}|n_2\vec{k}\sigma'_z\rangle.
\end{aligned}
\tag{B.12}
$$

Finally, we diagonalize the full Hamiltonian matrix to obtain the eigenvalues and eigenvectors with spin-orbit coupling.

B.3. Results and Discussions

As shown in Table B.1, our calculations for spin-orbit splittings in Ge and GaAs agree with previous calculations and with experiment to within 20 meV. We include $V^{LOC}(r)$ and v^{ion}_{ℓ} in the ground state calculation and treat H_{so} perturbatively. After the ground state calculation, we apply H_{so} to the lowest n bands and diagonalize

TABLE B.1 Spin-orbit splittings in Ge and GaAs. In both materials, the spin-orbit splittings of the present calculations agree with previous calculations and with experiment within 20 meV. Ref. 9 uses a semi-local form for the pseudopotential. The present method and Ref. 10 use Kleinman-Bylander forms for both pseudopotentials with different forms for the ionic and spin-orbit pseudopotentials. We use 10 hartree for the energy cut-off of the plane-waves and 28 $\vec{k}$-points in the irreducible Brillouin zone for integration in the ground state calculations. All the units are meV.

Ge	Present	Ref. 9	Exp. (Ref. 15)	GaAs	Present	Ref. 10	Exp. (Ref. 16)
Γ_v	306	300	296±3	Γ_v	350	340	341±2
Γ_c	223	220	200±3	Γ_c	196	191	171±15
L_v	193	190	184±2	L_v	215	211	220±2
L_c	96	100		L_c	85		
				X_v	85	82	77±10

the $2n \times 2n$ matrix. We take $n = 50$ (about 2 hartree above the valence band edge) in the present calculation. We use norm-conserving pseudopotentials constructed using the method of Troullier and Martins.[13] We test calculations with both single- and double-reference states.[14] The spin-orbit splittings obtained with single- and double-reference states differ by less than 2 meV. The values reported are all from double-reference state calculations. When constructing the double-reference pseudopotential, the second-reference state energies are chosen to be 1 hartree above the first reference energies. In H_{so}, both $\ell = 1$ and 2 are included.

Having tested our method for Ge and GaAs, we carry out the spin-orbit calculations for 11 other semiconductors with cubic symmetry. Results listed in Table B.2 show good agreement between our calculations and available experiment. There are pronounced differences for AlSb and InP at the Γ point of the conduction band. Further studies using LMTO/LAPW calculations and experimental measurements are needed to clarify the origin of such large discrepancies.

Our method is easy to implement to existing plane-wave codes. For the ground state calculation, i.e., without spin-orbit coupling, the only change needed is adding multiple projection operators for the ionic pseudopotentials of the Kleinman-Bylander type. This feature is already present for many plane-wave codes. At the end of the ground state calculation, one needs to add a separate subroutine of about 200 lines to compute the spin-orbit Hamiltonian matrix followed by the diagonalization. With such minor changes, one gains the ability to calculating many properties that were previously unaccessible with the pseudopotential method.

In our current implementation, the spin-orbit coupling is calculated perturbatively using the electronic density of the non-split Hamiltonian. For row IV elements where the spin-orbit effects are large enough to change the densities, one needs to recompute the electronic density after obtaining the eigenvectors with the spin-orbit splitting. With the new density, one then recomputes the eigenstates of the non-split Hamiltonian. Next, one applies the spin-orbit Hamiltonian again perturbatively to obtain the new eigenstates and the new density. This process is continued until the eigenstates and the density have converged. For even heavier elements where the spin-orbit coupling is no longer a perturbation, one needs to treat the spin-orbit coupling with the same footing as the ionic potential. Such

TABLE B.2 Calculated spin-orbit splittings for 13 cubic semiconductors compared with exepriment. The values are reported for the valence (v) and conduction (c) bands at the $\vec{k}$-points Γ, X, and L. There is good agreement between our calculations and experiment. Two exceptions are at the Γ point of the conduction band of AlSb and InP. The origin of these discrepancies is unclear. The energy cut-off for the plane-waves are chosen to be 10 hartree except for GaN and InN where it is 25 hartree. The number of $\vec{k}$-points used is 28 in the irreducible Brillouin zone. Units are in meV.

	Present calculation					Experiment				
	Γ		L		X	Γ		L		X
	v	c	v	c	v	v	c	v	c	v
Si	52	39	34	17		44				
Ge	306	223	193	96		296	200	184		
AlP	63	31	40	14	19					
AlAs	311	38	180	20	129	275		200		150
AlSb	743	51	417	35	323	750	300			
GaN	9	332	27	129	56					
GaP	90	177	73	67	23	80				
GaAs	350	196	215	85	85	341	171	220	77	
GaSb	795	208	457	108	292	760	200			
InN	21	795	61	309	134					
InP	121	483	125	189	102	108	70			
InAs	376	493	272	197	1	380		267		
InSb	813	451	512	198	214	810	390			

calculations require doubling of the basis functions to add the spin indices of up and down for the ground state calculation. Needless to say, such calculations are more demanding numerically.

Another direction to extend the current work is to calculate the optical response including the spin-orbit coupling. One needs to include the term $[\vec{r}, H_{so}]$ to the momentum operator for such calculations. The first-order correction to the optical response from the spin-orbit coupling vanishes because the non-spin-split calculation is the weighted average of the spin-split one. So the leading spin-orbit correction to optical response is second-order. Nevertheless, the spin-orbit correction to the dielectric constant for GaAs is a few percent[17] because the spin-orbit splitting at Γ is 0.35 eV whereas the gap is 1.5 eV. The spin-orbit effects should have a larger correction to the second-harmonic susceptibility which depends more sensitively on the gap and the momentum matrix elements [cf. Eq. (2.46)].

B.4. Summary

We propose a new method to calculate the spin-orbit coupling with Kleinman-Bylander type pseudopotentials. The functional form of our proposed pseudopotentials are simpler and easier to derive than a previously proposed method.[10] Our calculated spin-orbit splittings for group IV and III-V compounds agree with previous calculations and with experiment. Noticeable discrepancies are at the Γ point of the conduction band in AlSb and InP where our calculated spin-orbit splittings are significantly different from experimental values. Calculations using other methods and more experimental measurements are needed to clarify these discrepancies.

APPENDIX C
COMPARISON OF THE "$2n + 1$" AND SUM-OVER-STATES METHODS FOR SECOND-HARMONIC SUSCEPTIBILITY

C.1. Introduction

A new method[18] was recently proposed to calculate the second-harmonic susceptibility using the "$2n + 1$" theorem. The "$2n + 1$" theorem states[19,18] the derivatives of the energy to order $2n + 1$ can be computed if the change of the wave function is known up to order n. The case of $n = 1$ applies to calculating the second-harmonic susceptibility which is the third derivative of the energy. The new expression given by the "$2n + 1$" method is more compact than the one given by the sum-over-states method. The new expression has no explicit dependence on the conduction bands, which eliminates the diagonalization of the Hamiltonian matrix required in the sum-over-states method. Using the "$2n+1$" method, the computer time needed to calculate the second-harmonic susceptibility is only a few times that of the LDA ground state calculation.[18] Thus it has the potential of applying to larger systems.

In this Appendix, we prove that although the expressions obtained using the "$2n+1$" method and the sum-over-states method appear to be different, they are analytically equivalent. Furthermore, we show that the "scissors-operator", which is applied in the sum-over-state method to give close aggreement with experiment, can be easily incorporated into the "$2n+1$" method despite the the fact that it has explicit dependence on only the valence bands. Calculations of the second-harmonic susceptibilities for the III-V semiconductors using the two methods with the same input parameters, i.e., lattice constants, energy cut-offs, and number of $\vec{k}$-points for integration, give very similar results, which provides further confirmation that the two methods are equivalent.

C.2. Classical Analogue

Prior to giving the new expression using the "$2n+1$" method, we provide an example of applying the "$2n+1$" theorem to a classical system to calculate the second-harmonic susceptibility $\chi^{(2)}$. The idea is to calculate the change in the energy to third-order in the external field, which is proportional to $\chi^{(2)}$. We will show that this third-order change in energy can be expressed by using only the first-order displacement. Terms involving the second-order displacement are canceled.

Consider a particle with unit charge in a one-dimensional potential $V(x)$ with its equilibrium position at $x = 0$. If an infinitesimal static electric field E is applied, the Hamiltonian of the system at its new equilibrium position reads

$$H(x) = V(x) - Ex. \tag{C.1}$$

We expand the Hamiltonian near $x = 0$ with the notation $V_n \equiv d^n V(x=0)/dx^n$

$$H(x) = V_0 + \frac{1}{2!}V_2 x^2 + \frac{1}{3!}V_3 x^3 + \cdots - Ex, \tag{C.2}$$

where $V_1 = 0$ because $V(x)$ is minimum at $x = 0$.

"Sum-over-states" method. The physical displacement x_s of the particle corresponds to the position where $H(x)$ is stationary, i.e.,

$$0 = \frac{\delta H(x = x_s)}{\delta x} = V_2 x_s + V_3 x_s^2/2 + \cdots - E. \tag{C.3}$$

Solving the above equation for x_s to second-order in E gives

$$x_s = E/V_2 - E^2 V_3/2V_2^3. \tag{C.4}$$

The linear and second-order nonlinear susceptibilities $\chi^{(1)}$ and $\chi^{(2)}$ are defined by

$$x_s \equiv \chi^{(1)}E + \chi^{(2)}E^2. \tag{C.5}$$

Comparing Eqs. (C.4) and (C.5) yields

$$\begin{aligned} \chi^{(1)} &= 1/V_2, \\ \chi^{(2)} &= -V_3/2V_2^3. \end{aligned} \tag{C.6}$$

The above procedure to calculate $\chi^{(2)}$ corresponds to the sum-over-states method in which the displacement to second-order in the external field is computed.

" $2n+1$ " method. Now we show why and how $\chi^{(2)}$ can be calculated using the "$2n+1$" method for this system. Replacing x in Eq. (C.2) by its stationary solution x_s in Eq. (C.5) gives the stationary Hamiltonian

$$\begin{aligned} &H_s(x_s) = V_0 + V_1 x_s^2/2 + V_3 x_s^3/6 + \cdots - Ex_s \\ =&V_0 + E^2\left[(\chi^{(1)})^2 V_2/2 - \chi^{(1)}\right] + E^3\left[V_3(\chi^{(1)})^3/6 + (V_2\chi^{(1)} - 1)\chi^{(2)}/2\right] + O(E^4) \\ =&V_0 - (\chi^{(1)}E)E/2 + (\chi^{(1)}E)^3 V_3/6 + O(E^4), \end{aligned} \tag{C.7}$$

where $\chi^{(1)} = 1/V_2$ given in Eq. (C.6) is used in the last step. Equation (C.7) shows that at the stationary solution, the change of the Hamiltonian up to the third-order in the external field can be expressed in terms of $\chi^{(1)}E$ – the first-order displacement. The coefficient in front of $\chi^{(2)}$ in Eq. (C.7) is canceled at the second equal sign. From Eq. (C.7), we can obtain $\chi^{(2)}$ by taking the third derivative of the stationary Hamiltonian with respect to the external field

$$\chi^{(2)} = -\frac{1}{2}\partial^3 H_s/\partial E^3 = -(\chi^{(1)})^3 V_3/2 = -V_3/2V_2^2, \tag{C.8}$$

the result is identical to Eq. (C.6). Equations (C.7) and (C.8) give the essence of the "$2n+1$" method to calculate $\chi^{(2)}$: after obtaining the first-order displacement of the particle, the third-order change of the energy can be calculated which is directly proportional to $\chi^{(2)}$.

The sum-over-states method of calculating $\chi^{(2)}$ corresponds to solving Eq. (C.3) in which the displacement to second-order in the external field is computed. In a quantum mechanical calculation for $\chi^{(2)}$, the second-order change of the wavefunction needs be calculated which is more involved than calculating the first-order change. The "$2n + 1$" method avoids calculating the second-order change of the wavefunction by computing the change of the energy to third-order from the first-order change of the wavefunction. The resulting expression is simpler and easier to evaluate numerically.

C.3. Quantum expression for the second-harmonic susceptibility of the "$2n+1$" method

In this section, we give the expression for the second-harmonic susceptibility obtained using the "$2n+1$" theorem. A formula was first derived in the Wannier representation consisting of the ground state and the first-order change of the wavefunctions and the $\hat{r}$ operator.[18] This formula was then cast in the Bloch representation in the reciprocal space at which the numerical calculation is performed. We only give the final expression in the Bloch representation. The notation is changed slightly from Ref. 18 for easier comparison with the sum-over-states method described in Chapter 2.

In the "$2n+1$" method, the external electric field is represented by a scalar potential

$$\begin{gathered} V_{ext}(\vec{r},t,\vec{a}) = a_1\vec{e}_1\cdot\vec{r}\cos(\omega_1 t) + a_2\vec{e}_2\cdot\vec{r}\cos(\omega_2 t) + a_3\vec{e}_3\cdot\vec{r}\cos(\omega_3 t), \\ \vec{e}_i : \text{unit vectors}, \qquad a_i : \text{strength of the electric fields}. \end{gathered} \tag{C.9}$$

The case $\omega_2 = \omega_3 = \omega$, $\omega_1 = 2\omega$ applies to the calculation of the second-harmonic susceptibility. The ground state eigenstates and eigenvalues are denoted by $|u_{m\vec{k}}\rangle$ and $\epsilon_{m\vec{k}}$, respectively. The first-order change of the wavefunctions $|u^{a_1\pm}_{m\vec{k}}\rangle$ can be computed using perturbation theory in the presence of an external field (with unit strength) $\vec{e}_1\cdot\vec{r}\cos(\omega_1 t)$ and the linear local field $\phi^{(1)}_{a_1}(\vec{r},t)$. With $|u^{a_1\pm}_{m\vec{k}}\rangle$, one then constructs the linearly induced short-wave density $n^{(1)}_{a_1}(\vec{r},t)$. The linear local field is related to the $n^{(1)}_{a_1}(\vec{r},t)$ via the Hartree and exchange-correlation potentials. The relation between these quantities – the change of the wavefunctions, density, and local field – are summarized by the following coupled equations:

$$
\begin{aligned}
(\epsilon_{m\vec{k}} - H_0 \pm \omega_1)|u^{a_1\pm}_{m\vec{k}}\rangle &= Q_{\vec{k}}\left(\frac{\vec{e}_1\cdot\vec{r}}{2} + \frac{\phi^{(1)}_{a_1}(\vec{r})}{2}\right)|u_{m\vec{k}}\rangle, \\
Q_{\vec{k}} &= \vec{1} - \sum_m^v |u_{m\vec{k}}\rangle\langle u_{m\vec{k}}|, \\
n^{(1)}_{a_1}(\vec{r},t) &= 2\sum_m^v \sum_{\pm}\int_{BZ}\frac{d^3k}{(2\pi)^3} Re\left[\langle u_{m\vec{k}}|\vec{r}\rangle\langle\vec{r}|u^{a_1\pm}_{m\vec{k}}\rangle\right], \\
\phi^{(1)}_{a_1}(\vec{r},t) &= \int d^3r'\left[\frac{1}{|\vec{r}-\vec{r}\,'|} + \frac{\delta V_{xc}[n(\vec{r}\,')]}{\delta n(\vec{r}\,')}\delta(\vec{r}-\vec{r}\,')\right] n^{(1)}_{a_1}(\vec{r}\,',t),
\end{aligned}
\tag{C.10}
$$

where $Q_{\vec{k}}$ is the projection operator onto the conduction bands. The final expression for the second-order susceptibility is

$$
\begin{aligned}
&\chi^{(2)}_{\vec{e}_1;\vec{e}_2,\vec{e}_3}(-\omega_1;\omega_2,\omega_3) \\
&= -2\sum_{m,n}^v\sum_{\pm}\int_{BZ}\frac{d^3k}{(2\pi)^3}\Big[\langle u_{m\vec{k}}|\frac{\vec{e}_2}{2}\cdot\frac{-i\partial}{\partial\vec{k}}\left(|u_{n\vec{k}}\rangle\langle u^{a_1\mp}_{n\vec{k}}|\right)|u^{a_3\pm}_{m\vec{k}}\rangle \\
&+ \delta_{m,n}\langle u^{a_1\mp}_{n\vec{k}}|\phi^{(1)}_{a_2}|u^{a_3\pm}_{m\vec{k}}\rangle - \langle u_{m\vec{k}}|\phi^{(1)}_{a_2}|u_{n\vec{k}}\rangle\langle u^{a_1\mp}_{n\vec{k}}|u^{a_3\pm}_{m\vec{k}}\rangle\Big] \\
&- \frac{1}{12}\int d^3r d^3r' d^3r'' K_{xc}(\omega_2,\omega_3,\vec{r},\vec{r}\,',\vec{r}\,'')n^{(1)}_{a_1}(\vec{r})n^{(1)}_{a_2}(\vec{r}\,')n^{(1)}_{a_3}(\vec{r}\,'') \\
&+ (\text{permutations of } 1,2,3),
\end{aligned}
\tag{C.11}
$$

where

$$
K_{xc}(\omega_2,\omega_3,\vec{r},\vec{r}\,',\vec{r}\,'') = \int_0^T dt'\int_0^T dt\frac{\delta A_{xc}[n^0]}{\delta n(\vec{r},0)\delta n(\vec{r}\,',t')\delta n(\vec{r}\,'',t)}e^{i\omega_2 t'}e^{i\omega_3 t}.
$$

Notice that the sums over n and m are both over valence bands. The dependence on the conduction bands are implicit in $|u^{a_1\pm}_{m\vec{k}}\rangle$ and the derivative of $\vec{k}$. We will show in the next section that when these dependencies on the conduction bands are written out explicitly, Eq. (C.11) is equivalent to Eq. (2.39) of the sum-over-states method given in Chapter 2.

C.4. Analytical proof of equivalence of the "$2n+1$" method and the sum-over-states method

To prove that the "$2n+1$" method and the sum-over-states method are equivalent analytically, we first rewrite Eq. (C.11) using the explicit dependence of $|u^{a_1\pm}_{m\vec{k}}\rangle$ and $\partial/\partial\vec{k}$ on the conduction bands. Next we collect the resulting terms into ccv (i.e., $\sum_m^v \sum_j^c \sum_l^c$) and vvc (i.e., $\sum_m^v \sum_n^v \sum_l^c$) contributions which will be shown to be identical to the corresponding contributions from the sum-over-states method given in Sec. 2.8. For simplicity, we neglect the terms containing $H^{(2)} \equiv \nabla_{\vec{k}}\nabla_{\vec{k}}H_{\vec{k}}/2$ and suppress the directions on the velocity operator $H^{(1)}$ and the local field $\phi^{(1)}$, which corresponds to scalar response.

We can express the first-order change of the wavefunction $|u^{a_1\pm}_{m\vec{k}}\rangle$ in Eq. (C.10) formally in terms of the conduction bands,

$$
\begin{aligned}
|u^{a_1\pm}_{m\vec{k}}\rangle &= (\epsilon_{m,\vec{k}} - H_0 \pm \omega_1)^{-1} Q_{\vec{k}} \left(\frac{\vec{e}_1\cdot\vec{r}}{2} + \frac{\phi^{(1)}_{a_1}}{2} \right) |u_{m\vec{k}}\rangle. \\
&= \frac{1}{2}\sum_l^c \frac{|u_{l\vec{k}}\rangle\langle u_{l\vec{k}}|\vec{e}_1\cdot\vec{r} + \phi^{(1)}_{a_1}|u_{m\vec{k}}\rangle}{\epsilon_{m\vec{k}} - \epsilon_{l\vec{k}} \pm \omega_1} \\
&= \frac{1}{2}\sum_l^c i\frac{|u_{l\vec{k}}\rangle\langle u_{l\vec{k}}|\vec{e}_1\cdot\vec{H}^{(1)}|u_{m\vec{k}}\rangle}{(\epsilon_{m\vec{k}} - \epsilon_{l\vec{k}} \pm \omega_1)(\epsilon_{m\vec{k}} - \epsilon_{l\vec{k}})} + \frac{|u_{l\vec{k}}\rangle\langle u_{l\vec{k}}|\phi^{(1)}_{a_1}|u_{m\vec{k}}\rangle}{\epsilon_{m\vec{k}} - \epsilon_{l\vec{k}} \pm \omega_1}.
\end{aligned}
\tag{C.12}
$$

At the third equal sign, the following identity is used,

$$
\langle u_{c\vec{k}}|r|u_{v\vec{k}}\rangle = i\langle u_{c\vec{k}}|H^{(1)}|u_{v\vec{k}}\rangle/(\epsilon_{v\vec{k}} - \epsilon_{c\vec{k}}). \tag{C.13}
$$

For the partial derivative $\partial/\partial k$, we can use $\vec{k}\cdot\vec{p}$ perturbation theory to give

$$
\begin{aligned}
\frac{\partial}{\partial\vec{k}}|u_{m\vec{k}}\rangle &= \sum_{l\neq m} \frac{|u_{l\vec{k}}\rangle\langle u_{l\vec{k}}|\vec{H}^{(1)}|u_{m\vec{k}}\rangle}{\epsilon_{m\vec{k}} - \epsilon_{l\vec{k}}}, \\
\frac{\partial}{\partial\vec{k}}\epsilon_{m\vec{k}} &= |m\vec{k}\rangle\langle m\vec{k}|H^{(1)}|m\vec{k}\rangle.
\end{aligned}
\tag{C.14}
$$

Equations (C.12), (C.13), and (C.14) are the keys to connect the "$2n+1$" method and the sum-over-states method.

We concentrate on the long-wave contribution of Eq. (C.11) and ignore all local-field corrections (i.e., terms containing $n^{(1)}$ and $\phi^{(1)}$). Applying Eqs. (C12-14) using the short-hand notations $H^{(1)}_{nm} \equiv \langle u_{m\vec{k}}|H^{(1)}|u_{m\vec{k}}\rangle$, $\epsilon_{nm} \equiv \epsilon_{n\vec{k}} - \epsilon_{m\vec{k}}$ yields

$$
\begin{aligned}
\chi^{(2)}(-\omega_1;\omega_2,\omega_3) = & -2\sum_m^v\sum_n^v\sum_{\pm}\int_{BZ}\frac{d^3k}{(2\pi)^3}\Big\{\langle u_{m\vec{k}}|\Big[-\frac{i}{2}\frac{\partial}{\partial k}\Big(|u_{n\vec{k}}\rangle\langle u^{a_1\mp}_{n\vec{k}}|\Big)\Big]|u^{a_3\pm}_{m\vec{k}}\rangle\Big\} \\
& + \text{(permutations of 1,2,3)} \\
=&\frac{i}{4}\sum_m^v\sum_n^v\sum_{\pm}\int_{BZ}\frac{d^3k}{(2\pi)^3}\Big\{\langle u_{m\vec{k}}| \\
&\times\Big[\sum_{j\neq n}\sum_i^c\frac{|u_{j\vec{k}}\rangle H^{(1)}_{jn}}{\epsilon_{nj}}\frac{H^{(1)}_{ni}\langle u_{i\vec{k}}|}{\epsilon_{ni}(\epsilon_{ni}\mp\omega_1)}+\sum_i^c\sum_{j\neq n}\frac{|u_{n\vec{k}}\rangle H^{(1)}_{nj}H^{(1)}_{ji}\langle u_{i\vec{k}}|}{\epsilon_{nj}\epsilon_{ni}(\epsilon_{ni}\mp\omega)} \\
&+\sum_j^c\sum_{i\neq j}\frac{|u_{n\vec{k}}\rangle H^{(1)}_{ni}H^{(1)}_{ij}\langle u_{j\vec{k}}|}{\epsilon_{nj}(\epsilon_{nj}\mp\omega_1)\epsilon_{ji}}+\sum_j^c\sum_{i\neq j}\frac{|u_{n\vec{k}}\rangle H^{(1)}_{ni}H^{(1)}_{ij}\langle u_{j\vec{k}}|}{\epsilon_{ni}(\epsilon_{ni}\mp\omega_1)\epsilon_{ij}} \\
&+\sum_j^c\frac{(2\epsilon_{ni}\mp\omega_1)|u_{n\vec{k}}\rangle H^{(1)}_{ni}\Big(H^{(1)}_{ii}-H^{(1)}_{nn}\Big)\langle u_{i\vec{k}}|}{\epsilon^2_{ni}(\epsilon_{ni}\mp\omega_1)^2}\Big]\sum_l^c\frac{|u_{l\vec{k}}\rangle H^{(1)}_{lm}}{\epsilon_{ml}(\epsilon_{ml}\pm\omega_3)}\Big\} \\
&+\text{(permumations of 1,2,3)} \\
=&\frac{i}{4}\sum_{\pm}\int_{BZ}\frac{d^3k}{(2\pi)^3}\Big\{\sum_m^v\sum_{n\neq m}^v\sum_l^c\frac{H^{(1)}_{mn}H^{(1)}_{nl}H^{(1)}_{lm}}{\epsilon_{nm}\epsilon_{nl}(\epsilon_{nl}\mp\omega_1)\epsilon_{ml}(\epsilon_{ml}\pm\omega_3)} \\
&+\sum_m^v\sum_{j\neq m}\sum_l^c\frac{H^{(1)}_{mj}H^{(1)}_{jl}H^{(1)}_{lm}}{\epsilon_{mj}\epsilon^2_{ml}(\epsilon_{ml}\mp\omega_1)(\epsilon_{ml}\pm\omega_3)} \\
&+\sum_m^v\sum_{j\neq l}\sum_l^c\Big[\frac{H^{(1)}_{mj}H^{(1)}_{jl}H^{(1)}_{lm}}{\epsilon^2_{ml}(\epsilon_{ml}\mp\omega_1)\epsilon_{lj}(\epsilon_{ml}\pm\omega_3)}+\frac{H^{(1)}_{mj}H^{(1)}_{jl}H^{(1)}_{lm}}{\epsilon^2_{ml}(\epsilon_{ml}\mp\omega)\epsilon_{lj}(\epsilon_{ml}\pm\omega_3)}\Big] \\
&+\sum_m^v\sum_l^c\frac{(2\epsilon_{ml}\mp\omega_1)H^{(1)}_{ml}\Big(H^{(1)}_{ll}-H^{(1)}_{mm}\Big)H^{(1)}_{lm}}{\epsilon^3_{ml}(\epsilon_{ml}\mp\omega_1)^2(\epsilon_{ml}\pm\omega_3)}\Big\}+\text{(permutaions of 1,2,3)} \\
=&ccv+vvc,
\end{aligned}
\tag{C.15}
$$

in which the ccv and vvc contributions are

$$
\begin{aligned}
ccv =& \frac{i}{4}\sum_{\pm}\int_{BZ}\frac{d^3k}{(2\pi)^3}\Bigg\{\sum_{m}^{v}\sum_{j}^{c}\sum_{l}^{c}\frac{H_{mj}^{(1)}H_{jl}^{(1)}H_{lm}^{(1)}}{\epsilon_{mj}\epsilon_{ml}^2(\epsilon_{ml}\mp\omega_1)(\epsilon_{ml}\pm\omega_3)} \\
&+\sum_{m}^{v}\sum_{j\neq l}^{c}\sum_{l}^{c}\left[\frac{H_{mj}^{(1)}H_{jl}^{(1)}H_{lm}^{(1)}}{\epsilon_{ml}^2(\epsilon_{ml}\mp\omega_1)\epsilon_{lj}(\epsilon_{ml}\pm\omega_3)}+\frac{H_{mj}^{(1)}H_{jl}^{(1)}H_{lm}^{(1)}}{\epsilon_{mj}(\epsilon_{mj}\mp\omega)\epsilon_{jl}\epsilon_{ml}(\epsilon_{ml}\pm\omega_3)}\right] \\
&+\sum_{m}^{v}\sum_{l}^{c}\frac{(2\epsilon_{ml}\mp\omega_1)H_{ml}^{(1)}H_{ll}^{(1)}H_{lm}^{(1)}}{\epsilon_{ml}^3(\epsilon_{ml}\mp\omega_1)^2(\epsilon_{ml}\pm\omega_3)}\Bigg\}+\text{(permutations of 1,2,3)},
\end{aligned}
\tag{C.16}
$$

and

$$
\begin{aligned}
vvc =& \frac{i}{4}\sum_{\pm}\int_{BZ}\frac{d^3k}{(2\pi)^3}\Bigg\{\sum_{m}^{v}\sum_{n}^{v}\sum_{l}^{c}\frac{H_{mn}^{(1)}H_{nl}^{(1)}H_{lm}^{(1)}}{\epsilon_{ml}^2(\epsilon_{ml}\mp\omega_1)\epsilon_{ln}(\epsilon_{ml}\pm\omega_3)} \\
&+\sum_{m}^{v}\sum_{n\neq m}^{v}\sum_{l}^{c}\left[\frac{H_{mn}^{(1)}H_{nl}^{(1)}H_{lm}^{(1)}}{\epsilon_{nm}\epsilon_{nl}(\epsilon_{nl}\mp\omega_1)\epsilon_{ml}(\epsilon_{ml}\pm\omega_3)}+\frac{H_{mn}^{(1)}H_{nl}^{(1)}H_{lm}^{(1)}}{\epsilon_{mn}\epsilon_{ml}^2(\epsilon_{ml}\mp\omega_1)(\epsilon_{ml}\pm\omega_3)}\right] \\
&-\sum_{m}^{v}\sum_{l}^{c}\frac{(2\epsilon_{ml}\pm\omega_1)H_{ml}^{(1)}H_{mm}^{(1)}H_{lm}^{(1)}}{\epsilon_{ml}^3(\epsilon_{ml}\mp\omega_1)^2(\epsilon_{ml}\pm\omega_3)}\Bigg\}+\text{(permutations of 1,2,3)}.
\end{aligned}
\tag{C.17}
$$

The ccv and vvc contributions each have 24 terms after the permutations of 1, 2, and 3 are included. We simplify the ccv (vvc) contributions by symmetrizing with respect to the two conduction (valence) band indices j and l (m and n). After summing over the $\pm\vec{k}$ pairs and using the time reversal symmetry, the resulting 48 terms in the ccv and vvc can be simplified, using the symbolic manipulator Maple, to give

$$
\begin{aligned}
ccv =& \sum_{m}^{v}\sum_{j}^{c}\sum_{l}^{c}\int_{BZ}\frac{d^3k}{(2\pi)^3}\mathrm{Im}\left(H_{mj}^{(1)}H_{jl}^{(1)}H_{lm}^{(1)}\right) \\
&\times\frac{3}{2}\frac{\epsilon_{jl}\left(2\epsilon_{ml}^2+2\epsilon_{mj}^2+3\epsilon_{ml}\epsilon_{mj}-4\omega^2\right)}{(\epsilon_{mj}^2-4\omega^2)(\epsilon_{mj}^2-\omega^2)(\epsilon_{ml}^2-4\omega^2)(\epsilon_{ml}^2-\omega^2)},
\end{aligned}
\tag{C.18}
$$

and

$$vvc = \sum_{m}^{v}\sum_{n}^{v}\sum_{l}^{c}\int_{BZ}\frac{d^3k}{(2\pi)^3}\mathrm{Im}\left(H^{(1)}_{mn}H^{(1)}_{nl}H^{(1)}_{lm}\right) \times \frac{3}{2}\frac{\epsilon_{nm}\left(2\epsilon^2_{ml}+2\epsilon^2_{nl}+3\epsilon_{ml}\epsilon_{nl}-4\omega^2\right)}{(\epsilon^2_{ml}-4\omega^2)(\epsilon^2_{ml}-\omega^2)(\epsilon^2_{nl}-4\omega^2)(\epsilon^2_{nl}-\omega^2)}. \tag{C.19}$$

Eqs. (C.18) and (C.19) are identical to Eqs. (2.49) and (2.50) of the ccv and vvc contributions (with $\omega = 0$) of the sum-over-states method (after Eq. (2.49) is symmetrized with respect to the conduction band indices). We have thus proved that the long-wave contributions from the "$2n+1$" method and the sum-over-states method are equivalent. The equivalence of the local-field contributions of the two different methods can be proved analogously.

C.5. Scissors-operator in the "$2n+1$" method

The over-estimation of optical response coefficients using the local-density approximation (LDA) is argued in Sec. 1.5 to be associated with the small LDA band gap. The "scissors-operator" approach was introduced in to shift the conduction band energies from the small LDA values to the experimental ones.[20] Optical response calculations including the dielectric constants, the second-harmonic susceptibilities, and optical activity coefficients using the scissors-operator was implemented in the sum-over-states method and gives close agreement with experiment. In this section, we show that the scissors-operator can be easily applied in the "$2n+1$" method despite the fact that it has explicit dependence on only the valence bands.

To include the scissors-operator in the "$2n+1$" method, the only modification is to the first expression in Eq. (C.10) for the first-order change of the wavefunction

$$(\epsilon_{m\vec{k}} - H_0 - \Delta \pm \omega_1)|u^{a_1\pm}_{m\vec{k}}\rangle = Q_{\vec{k}} \left(\frac{\vec{e}_1 \cdot \vec{r}}{2} + \frac{\phi^{(1)}_{a_1}(\vec{r})}{2} \right) |u_{m\vec{k}}\rangle, \tag{C.20}$$

where the shift of the conduction band energies Δ is inserted on the left hand side of the equation. The other expressions in Eqs. (C.10) and (C.11) remain intact. The shift Δ should appear at the same positions at the light frequency ω so that it gives the electron a higher barrier for the transitions. Other quantities in Eq. (C.11), such as the r operator and the implicit $\partial/\partial\vec{k}$, are the same for a band structure differing from the original band structure by only a shift in the conduction band energies.

Here, we give a direct proof that using Eq. (C.20) yields the same expression for $\chi^{(2)}$ as the scissors-operator form of the sum-over-states method. In particular, we examine only the long-wave contribution. The local-field corrections can be proved similarly. From Eq. (C.20), the first-order change of the wavefunction in terms of the conduction bands is

$$\begin{aligned}
|u^{a_1\pm}_{m\vec{k}}\rangle &= (\epsilon_{m,\vec{k}} - H_0 - \Delta \pm \omega_1)^{-1} Q_{\vec{k}} \left(\frac{\vec{e}_1 \cdot \vec{r}}{2} + \frac{\phi^{(1)}_{a_1}}{2} \right) |u_{m\vec{k}}\rangle. \\
&= \frac{1}{2} \sum_l^c \frac{|u_{l\vec{k}}\rangle\langle u_{l\vec{k}}|\vec{e}_1 \cdot \vec{r} + \phi^{(1)}_{a_1}|u_{m\vec{k}}\rangle}{\epsilon_{m\vec{k}} - \epsilon_{l\vec{k}} - \Delta \pm \omega_1} \\
&= \frac{1}{2} \sum_l^c i \frac{|u_{l\vec{k}}\rangle\langle u_{l\vec{k}}|\vec{e}_1 \cdot \vec{H}^{(1)}|u_{m\vec{k}}\rangle}{(\epsilon_{m\vec{k}} - \epsilon_{l\vec{k}} - \Delta \pm \omega_1)(\epsilon_{m\vec{k}} - \epsilon_{l\vec{k}})} + \frac{|u_{l\vec{k}}\rangle\langle u_{l\vec{k}}|\phi^{(1)}_{a_1}|u_{m\vec{k}}\rangle}{\epsilon_{m\vec{k}} - \epsilon_{l\vec{k}} - \Delta \pm \omega_1}.
\end{aligned} \tag{C.21}$$

Analogous to the steps in obtaining Eq. (C.16) and (C.17), substituting $|u^{a_1\pm}_{m\vec{k}}\rangle$ in Eq. (C.11) by Eq. (C.21), keeping only the long-wave contribution gives

$$
\begin{aligned}
\chi^{(2)}(-\omega_1;\omega_2,\omega_3) = & -2\sum_m^v\sum_n^v\sum_\pm\int_{BZ}\frac{d^3k}{(2\pi)^3}\Big\{\langle u_{m\vec{k}}|\Big[-\frac{i}{2}\frac{\partial}{\partial k}\Big(|u_{n\vec{k}}\rangle\langle u^{a_1\mp}_{n\vec{k}}|\Big)\Big]|u^{a_3\pm}_{m\vec{k}}\rangle\Big\} \\
& + \text{(permutations of 1,2,3)} \\
= & \frac{i}{4}\sum_m^v\sum_n^v\sum_\pm\int_{BZ}\frac{d^3k}{(2\pi)^3}\Big\{\langle u_{m\vec{k}}| \\
& \Big[\sum_{j\neq n}\sum_i^c\frac{|u_{j\vec{k}}\rangle H^{(1)}_{jn}}{\epsilon_{nj}}\frac{H^{(1)}_{ni}\langle u_{i\vec{k}}|}{\epsilon_{ni}(\epsilon_{ni}-\Delta\mp\omega_1)}+\sum_i^c\sum_{j\neq n}\frac{|u_{n\vec{k}}\rangle H^{(1)}_{nj}H^{(1)}_{ji}\langle u_{i\vec{k}}|}{\epsilon_{nj}\epsilon_{ni}(\epsilon_{ni}-\Delta\mp\omega)} \\
& +\sum_i^c\sum_{j\neq i}\frac{|u_{n\vec{k}}\rangle H^{(1)}_{nj}H^{(1)}_{ji}\langle u_{i\vec{k}}|}{\epsilon_{ni}(\epsilon_{ni}-\Delta\mp\omega_1)\epsilon_{ij}}+\sum_j^c\sum_{i\neq j}\frac{|u_{n\vec{k}}\rangle H^{(1)}_{nj}H^{(1)}_{ji}\langle u_{i\vec{k}}|}{\epsilon_{nj}(\epsilon_{nj}-\Delta\mp\omega_1)\epsilon_{ji}} \\
& +\sum_j^c\frac{(2\epsilon_{ni}-\Delta\mp\omega_1)|u_{n\vec{k}}\rangle H^{(1)}_{ni}\Big(H^{(1)}_{ii}-H^{(1)}_{nn}\Big)\langle u_{i\vec{k}}|}{\epsilon^2_{ni}(\epsilon_{ni}-\Delta\mp\omega_1)^2}\Big]\sum_l^c\frac{|u_{l\vec{k}}\rangle H^{(1)}_{lm}}{\epsilon_{ml}(\epsilon_{ml}-\Delta\pm\omega_3)}\Big\} \\
& + \text{(permutations of 1,2,3)} \\
= & \frac{i}{4}\sum_\pm\int_{BZ}\frac{d^3k}{(2\pi)^3}\Big\{\sum_m^v\sum_{n\neq m}^v\sum_l^c\frac{H^{(1)}_{mn}H^{(1)}_{nl}H^{(1)}_{lm}}{\epsilon_{nm}\epsilon_{nl}(\epsilon_{nl}-\Delta\mp\omega_1)\epsilon_{ml}(\epsilon_{ml}-\Delta\pm\omega_3)} \\
& +\sum_m^v\sum_{j\neq m}\sum_l^c\frac{H^{(1)}_{mj}H^{(1)}_{jl}H^{(1)}_{lm}}{\epsilon_{mj}\epsilon^2_{ml}(\epsilon_{ml}-\Delta\mp\omega_1)(\epsilon_{ml}-\Delta\pm\omega_3)} \\
& +\sum_m^v\sum_{j\neq l}\sum_l^c\frac{H^{(1)}_{mj}H^{(1)}_{jl}H^{(1)}_{lm}}{\epsilon^2_{ml}(\epsilon_{ml}-\Delta\mp\omega_1)\epsilon_{lj}(\epsilon_{ml}-\Delta\pm\omega_3)} \\
& +\sum_m^v\sum_{j\neq l}^c\sum_l^c\frac{H^{(1)}_{mj}H^{(1)}_{jl}H^{(1)}_{lm}}{\epsilon_{mj}(\epsilon_{mj}-\Delta\mp\omega)\epsilon_{jl}\epsilon_{ml}(\epsilon_{ml}-\Delta\pm\omega_3)} \\
& +\sum_m^v\sum_l^c\frac{(2\epsilon_{ml}-\Delta\mp\omega_1)H^{(1)}_{ml}\Big(H^{(1)}_{ll}-H^{(1)}_{mm}\Big)H^{(1)}_{lm}}{\epsilon^3_{ml}(\epsilon_{ml}-\Delta\mp\omega_1)^2(\epsilon_{ml}-\Delta\pm\omega_3)}\Big\} \\
& + \text{(permutations of 1,2,3)} \\
= & ccv + vvc,
\end{aligned}
\tag{C.22}
$$

in which the *ccv* and *vvc* contributions are

$$ccv = \frac{i}{4}\sum_{\pm}\int_{BZ}\frac{d^3k}{(2\pi)^3}\Bigg\{\sum_m^v\sum_j^c\sum_l^c\frac{H^{(1)}_{mj}H^{(1)}_{jl}H^{(1)}_{lm}}{\epsilon_{mj}\epsilon^2_{ml}(\epsilon_{ml}-\Delta\mp\omega_1)(\epsilon_{ml}-\Delta\pm\omega_3)}$$
$$+\sum_m^v\sum_{j\neq l}^c\sum_l^c\frac{H^{(1)}_{mj}H^{(1)}_{jl}H^{(1)}_{lm}}{\epsilon^2_{ml}(\epsilon_{ml}-\Delta\mp\omega_1)\epsilon_{lj}(\epsilon_{ml}-\Delta\pm\omega_3)}$$
$$+\sum_m^v\sum_{j\neq l}^c\sum_l^c\frac{H^{(1)}_{mj}H^{(1)}_{jl}H^{(1)}_{lm}}{\epsilon_{mj}(\epsilon_{ml}-\Delta\mp\omega)\epsilon_{jl}\epsilon_{ml}(\epsilon_{ml}-\Delta\pm\omega_3)}$$
$$+\sum_m^v\sum_l^c\frac{(2\epsilon_{ml}-\Delta\pm\omega_1)H^{(1)}_{ml}H^{(1)}_{ll}H^{(1)}_{lm}}{\epsilon^3_{ml}(\epsilon_{ml}-\Delta\mp\omega_1)^2(\epsilon_{ml}-\Delta\pm\omega_3)}\Bigg\}$$
$$+\,(\text{permutations of }1,2,3), \tag{C.23}$$

and

$$vvc = \frac{i}{4}\sum_{\pm}\int_{BZ}\frac{d^3k}{(2\pi)^3}\Bigg\{\sum_m^v\sum_{n\neq m}^v\sum_l^c\frac{H^{(1)}_{mn}H^{(1)}_{nl}H^{(1)}_{lm}}{\epsilon_{nm}\epsilon_{nl}(\epsilon_{nl}-\Delta\mp\omega_1)\epsilon_{ml}(\epsilon_{ml}-\Delta\pm\omega_3)}$$
$$+\sum_m^v\sum_{n\neq m}^v\sum_l^c\frac{H^{(1)}_{mn}H^{(1)}_{nl}H^{(1)}_{lm}}{\epsilon_{mn}\epsilon^2_{ml}(\epsilon_{ml}-\Delta\mp\omega_1)(\epsilon_{ml}-\Delta\pm\omega_3)}$$
$$+\sum_m^v\sum_n^v\sum_l^c\frac{H^{(1)}_{mn}H^{(1)}_{nl}H^{(1)}_{lm}}{\epsilon^2_{ml}(\epsilon_{ml}-\Delta\mp\omega_1)\epsilon_{ln}(\epsilon_{ml}-\Delta\pm\omega_3)}$$
$$-\sum_m^v\sum_l^c\frac{(2\epsilon_{ml}-\Delta\pm\omega_1)H^{(1)}_{ml}H^{(1)}_{mm}H^{(1)}_{lm}}{\epsilon^3_{ml}(\epsilon_{ml}-\Delta\mp\omega_1)^2(\epsilon_{ml}-\Delta\pm\omega_3)}\Bigg\}$$
$$+\,(\text{permutations of }1,2,3). \tag{C.24}$$

After including the permutations of 1, 2, and 3 for the *ccv* (*vvc*) terms, the conduction (valence) band indices can be symmetrized. The resulting expression for the *ccv* and *vvc* contribution can be shown, using Maple, to be identical to the *ccv* [Eq. (2.56)] and *vvc* [Eq. (2.57)] terms of the sum-over-states method in Chapter II after the conduction and valence band indices are symmetrized and the use of time-reversal symmetry. The procedure is not repeated here because of its length.

C.6. Numerical Results

We have proved in the previous sections that the "$2n+1$" and the sum-over-states methods are equivalent analytically. In this section we carry out numerical studies to further confirm that the two methods are equivalent. There are two sets of calculations conducted using the "$2n+1$" method:[18] (1) without nonlinear core-charge correction (NLCC) for the pseudopotentials,[21] and (2) with NLCC for the pseudopotentials. Here, for the sake of comparison, we carry out two sets of calculations just as in the calculations using the "$2n+1$" method. We use the same parameters as in the calculation of the "$2n+1$" method including the lattice constant, energy cut-off for the plane-waves, and the number of special $\vec{k}$-points for integration.

Results for calculations without NLCC for the pseudopotentials are shown in Table C.1. The calculated second-harmonic susceptibilities $d = \chi^{(2)}/2$ using the two different methods are in close agreement with each other. Table C.2 shows calculations with NLCC for the pseudopotentials. For GaP, GaAs, and InP, the calculated d values using the two different methods are very close. However for GaSb, the difference is large. We believe this large difference in GaSb comes from the difference in the band gaps of the two calculations which might come from the different choice of the pseudopotentials. In both Tables C.1 and C.2, the calculated dielectric constants of the calculations using the two different methods are also in good agreement with each other with again the exception of GaSb. Note that for GaSb, the spin-orbit coupling is 0.5 eV at the valence band edge, which is larger than the LDA band gap. So the spin-orbit coupling will have an important effect on the optical response results which is neglected in both calculations. We point

TABLE C.1 Comparison of the "$2n+1$" method and the sum-over-states (SOS) method for LDA calculations of the second-harmonic susceptibility $d = \chi^{(2)}/2$ using pseudopotentials without nonlinear core corrections.[21] In the SOS calculations, we use the same lattice constants as the "$2n+1$" calculations which correspond to the minimum of the LDA total energy. The band gaps, dielectric constants ε_∞ and d from the two different calculations are in good agreement with each other. The same input parameters are used for both calculations for better comparison of the methods: (1) the energy cut-off for the plane-waves is 12 hartree; (2) the number of special $\vec{k}$-points for integration is 28 in the irreducible Brillouin zone.

	Lattice Const.		Band Gap (eV)			ε_∞			d (pm/V)		
	LDA	Exp.	$2n+1$	SOS	Exp.	$2n+1$	SOS	Exp.	$2n+1$	SOS	Exp.
AlP	10.19	10.33	3.5	3.4	3.6	8.2	8.3	7.5	20	20	
AlAs	10.56	10.69	2.2	2.1	3.1	9.3	9.4	8.2	32	33	
GaP	10.01	10.28	2.8	2.6	2.9	9.8	9.9	9.0	34	36	37
GaAs	10.40	10.68	1.3	1.1	1.5	11.9	12.3	10.9	79	87	83

out that to make real predictions of optical response, the lattice constant at which the calculations are carried out should be the experimental ones which provide the physical electronic density.

C.7. Conclusions

We have shown that the "$2n+1$" method of calculating the second-harmonic susceptibility is analytically equivalent to the sum-over-states method. Numerical calculations on the III-V compounds using similar input parameters give similar results. The "$2n{+}1$" method is simpler to derive analytically and faster to calculate numerically. More extensive tests need be carried out using the "$2n + 1$" method especially with light frequencies close to or larger than the band gap. As pointed out in Ref. 22, a different functional may be needed to calculate the first-order change of the wavefunction for numerical stability for these situations. We have also shown that the scissors-operator can be easily incorporated into the "$2n + 1$" method.

TABLE C.2 Comparison of the "$2n + 1$" method and the sum-over-states (SOS) method for LDA calculations for the second-harmonic susceptibility $d = \chi^{(2)}/2$ using pseudopotentials with nonlinear core-charge corrections.[21] The nonlinear core-charge correction improves the quality of the pseudopotentials as is evident from the LDA lattice constants for GaP and GaAs which are closer to experiment here than in Table C.1 in which the nonlinear core-charge correction is absent. With the exception of GaSb, the calculations show good agreement between the two methods. For GaSb, the calculated d of the two methods differ by 40%. We believe this is largely due to the difference in the band gaps of the two calculations. The difference in the pseudopotential generation procedure might be the cause of the this difference. The energy cut-off and the number of $\vec{k}$-points are the same as in Table C.1.

	Lattice Const.		Band Gap (eV)			ε_∞			d (pm/V)		
	LDA	Exp.	$2n+1$	SOS	Exp.	$2n+1$	SOS	Exp.	$2n+1$	SOS	Exp.
GaP	10.12	10.28	2.0	2.2	2.9	10.0	10.2	9.0	42	44	37
GaAs	10.50	10.68	1.0	0.9	1.5	12.5	12.9	10.9	103	117	83
GaSb	11.37	11.49	0.5	0.2	0.8	16.7	19.1	14.4	308	517	419
InP	10.94	11.09	1.0	1.0	1.4	10.2	10.4	9.6	73	81	144

REFERENCES

1. D. J. Chadi and M. L. Cohen, Phys. Rev. B **8**, 5747 (1973).
2. H. J. Monkhorst and J. D. Pack, Phys. Rev. B **13**, 5188 (1976).
3. D. J. Chadi, Phys. Rev. B **16**, 1746 (1977); J. D. Pack and H. J. Monkhorst, *ibid.* **16**, 1748 (1977).
4. D. Gottlieb and S. A. Orszag, *Numerical analysis of spectral methods theory and applications,* (SIAM, Philadelphia, 1977), p. 26-28.
5. F. S. Acton, *Numerical Methods That Work,* (Harper & Row, New York, 1970), p.106.
6. Z. H. Levine and D. C. Allan, Phys. Rev. B **43**, 4187 (1991).
7. Z. H. Levine and D. C. Allan, Phys. Rev. B **44**, 12781 (1991).
8. G. B. Bachelet, D. R. Hamann, and M. Schlüter, Phys. Rev. B **25**, 2103 (1982).
9. M. S. Hybertsen and S. G. Louie, Phys. Rev. B **34**, 2920 (1986).
10. L. A. Hemstreet, C. Y. Fong, and J. S. Nelson, Phys. Rev. B **47**, 4238 (1993).
11. L. Kleinman and D. M. Bylander, Phys. Rev. Lett. **48**, 1425 (1982).
12. O. K. Andersen, Phys. Rev. B **12**, 3060 (1975).
13. N. Troullier and J. L. Martins, Phys. Rev. B **43**, 1993 (1991).
14. P. E. Blöchl, Phys. Rev. B **41**, 5414 (1990).
15. D. E. Aspnes, Phys. Rev. B **12**, 2997 (1975).
16. D. E. Aspnes, Phys. Rev. B **7**, 4605 (1973).
17. M. Alouani and J. M. Wills, Phys. Rev. B **54**, 2480 (1996).
18. A. Dal Corso and F. Mauri, Phys. Rev. B **50**, 5756 (1994); A. Dal Corso, F. Mauri, and A. Rubio, *ibid.* **53**, 15638 (1996).
19. X. Gonze and J. P. Vigneron, Phys. Rev. B **39**, 13120 (1989).
20. Z. H. Levine, and D. C. Allan, hys. Rev. Lett. **16**, 1719 (1989); Phys. Rev. B **43**, 4187 (1991).
21. S. G. Louie, S. Froyen, and M. L. Cohen, Phys. Rev. B **26**, 1738 (1982).
22. A. Pasquarello and Antonio Quattropani, Phys. Rev. B **48**, 5090 (1993).

BIBLIOGRAPHY

[1] F. S. Acton, *Numerical Methods That Work,* (Harper & Row, New York, 1970).

[2] S. L. Adler, Phys. Rev. **126**, 413 (1962).

[3] L. Akasaki and M. Hashimoto, Solid State Commun. **5**, 851 (1967).

[4] M. Alouani and J. M. Wills, Phys. Rev. B **54**, 2480 (1996).

[5] O. K. Andersen, Phys. Rev. B **12**, 3060 (1975).

[6] N. W. Ashcroft and N. D. Mermin, *Solid state physics,* (New York, Holt, Rinehart and Winston, 1976).

[7] D. E. Aspnes, Phys. Rev. B **6**, 4648 (1972).

[8] D. E. Aspnes, Phys. Rev. B **7**, 4605 (1973).

[9] D. E. Aspnes, Phys. Rev. B **12**, 2997 (1975).

[10] W. G. Aulbur, Z. H. Levine, J. W. Wilkins, and D. C. Allan, Phys. Rev. B **51**, 10691 (1995).

[11] W. G. Aulbur, L. Jönsson, and J. W. Wilkins, Phys. Rev. B, in print.

[12] G. B. Bachelet, D. R. Hamann, and M. Schlüter, Phys. Rev. B **25**, 2103 (1982).

[13] A. S. Barker and M. Ilegems, Phys. Rev. B **7**, 743 (1973).

[14] S. Baroni and R. Resta, Phys. Rev. B **33**, 7017 (1986).

[15] P. E. Blöchl, Phys. Rev. B **41**, 5414 (1990).

[16] N. Bloembergen, *Nonlinear optics,* (Benjamin, New York,) 1965.

[17] P. N. Butcher and T. P. McLean, Proc. Phys. Soc. (London) **81**, 219 (1963); **83**, 579 (1964).

[18] D. M. Ceperley and B. J. Alder, Phys. Rev. Lett. **45**, 566 (1980).

[19] D. J. Chadi, Phys. Rev. B **16**, 1746 (1977).

[20] D. J. Chadi and M. L. Cohen, Phys. Rev. B **8**, 5747 (1973).

[21] J. Chen, L. Jönsson, J. W. Wilkins, and Z. H. Levine, submitted to Phys. Rev. B.

[22] J. Chen, Z. H. Levine, and J. W. Wilkins, Phys. Rev. B **50**, 11514 (1994).

[23] J. Chen, Z. H. Levine, and J. W. Wilkins, Appl. Phys. Lett. **66**, 1129 (1995).

[24] N. E. Christensen and I. Gorczyca, Phys. Rev. B **50**, 4397 (1994).

[25] A. T. Collins, E. C. Lightowlers, and P. J. Dean, Phys. Rev. **158**, 833 (1967).

[26] A. Dal Corso, S. Baroni, and R. Resta, Phys. Rev. B **49**, 5323 (1994).

[27] A. Dal Corso and F. Mauri, Phys. Rev. B **50**, 5756 (1994).

[28] A. Dal Corso, F. Mauri, and A. Rubio, Phys. Rev. B **53**, 15638 (1996).

[29] V. G. Dmitriev, G. G. Gurzadyan, and D. N. Nidogosyan, *Handbook of nonlinear optical crystals,* (Springer-Verlag) 1991.

[30] C. Y. Fong and Y. R. Shen, Phys. Rev. B **12**, 2325 (1975).

[31] P. A. Franken, A. e. Hill, C. W. Peters, and G. Weinreich, Phys. Rev. Lett. **7**, 118 (1961).

[32] Y. Fujii, S. Yoshida, S. Misawa, S. Maekawa, and S. Sakudo, Appl. Phys. Lett. **31**, 815 (1978).

[33] E. Ghahramani, D. J. Moss, and J. E. Sipe, Phys. Rev. B **43**, 8990 (1991).

[34] W. Godby, M. Schlüter, and L. J. Sham, Phys. Rev. B **37**, 10159 (1988).

[35] X. Gonze and J. P. Vigneron, Phys. Rev. B **39**, 13120 (1989).

[36] X. Gonze, P. Käckell, and M. Scheffler, Phys. Rev. B **41**, 12264 (1990).

[37] X. Gonze, Ph. Ghosez, and R. W. Godby, Phys. Rev. Lett. **74**, 4035 (1995).

[38] D. Gottlieb and S. A. Orszag, *Numerical analysis of spectral methods theory and applications,* (SIAM, Philadelphia, 1977).

[39] D. R. Hamann, M. Schlüter, and C. Chiang, Phys. Rev. Lett. **43**, 1494 (1979).

[40] W. Hanke and L. J. Sham, Phys. Rev. B **12**, 4501 (1975).

[41] W. Hanke and L. J. Sham, Phys. Rev. B **21**, 4656 (1980).

[42] L. Hedin and S. Lundqvist, Solid State Phys. **23**, 1 (1969).

[43] Numerical Data and Functional Relationships in Science and Technology, edited by K.-H. Hellwege, Landolt-Bornstein Tables, Group III, Vol. 17a (Springer-Verlag, New York, 1982).

[44] L. A. Hemstreet, C. Y. Fong, and J. S. Nelson, Phys. Rev. B **47**, 4238 (1993).

[45] P. Hohenberg and W. Kohn, Phys. Rev. **136**, B864 (1964).

[46] M.-Z. Huang and W. Y. Ching, Phys. Rev. B **45**, 8738 (1992).

[47] M.-Z. Huang and W.-Y. Ching, Phys. Rev. B **47**, 9449 (1993).

[48] M. S. Hybertsen and S. G. Louie, Phys. Rev. B **34**, 5390 (1986).

[49] M. S. Hybertsen and S. G. Louie, Phys. Rev. B **35**, 5585 (1987).

[50] R. O. Jones and O. Gunnarsson, Rev. Mod. Phys. **61**, 689 (1989).

[51] L. Jönsson, Z. H. Levine, and J. W. Wilkins, Phys. Rev. Lett. **76**, 1372 (1996).

[52] R. D. King-Smith and D. Vanderbilt, Phys. Rev. B **47**, 1651 (1993).

[53] C. Kittel, *Quantum Theory of Solids*, New York, Wiley (1963).

[54] D. A. Kleinman, Phys. Rev. **128**, 1761 (1962).

[55] L. Kleinman and D. M. Bylander, Phys. Rev. Lett. **48**, 1425 (1982).

[56] W. Kohn and L. J. Sham, Phys. Rev. **140**, A1133 (1965).

[57] W. Kohn and P. Vashishta, *Theory of the inhomogeneous electron gas,* edited by S. Lundqvist and N. H. March, (Plenum Press, New York, 1983).

[58] W. R. L. Lambrecht, B. Segall, W. Suttrop, M. Yoganathan, R. R. Devaty, W. J. Choyke, J. A. Edmond, J. A. Powell, and M. Alouani, Appl. Phys. Lett. **63**, 2747 (1993).

[59] B. F. Levine, Phys. Rev. Lett. **25**, 440 (1970).

[60] B. F. Levine, Phys. Rev. B **7**, 2600 (1973).

[61] Z. H. Levine, and D. C. Allan, Phys. Rev. Lett. **16**, 1719 (1989).

[62] Z. H. Levine, Phys. Rev. B **42**, 3567 (1990).

[63] Z. H. Levine, and D. C. Allan, Phys. Rev. B **43**, 4187 (1991).

[64] Z. H. Levine and D. C. Allan, Phys. Rev. B **44**, 12781 (1991); **48**, 14768 (E) (1993).

[65] Z. H. Levine, Int. J. Quantum Chem. **S28**, 411 (1994).

[66] W. P. Liu, P. M. Lundquist, G. K. Wong, E. D. Rippert, and J. B. Ketterson, Appl. Phys. Lett. **63**, 2875 (1993).

[67] S. G. Louie, S. Froyen, and M. L. Cohen, Phys. Rev. B **26**, 1738 (1982).

[68] P. M. Lundquist, W. P. Lin, Z. Y. Xu, G. K. Wong, E. D. Rippert, J. A. Helfrich, and J. B. Ketterson, Appl. Phys. Lett. **65**, 1085 (1994).

[69] P. M. Lundquist, W. P. Lin, G. K. Wong, M. Razeghi, J. B. Ketterson, Appl. Phys. Lett. **66**, 1883 (1995).

[70] H. Ma, S. T. Chui, R. V. Kasowski, and W. Y. Hsu, Opt. comm, **85**, 437 (1991).

[71] R. M. Martin, Phys. Rev. B **9**, 1998 (1974).

[72] R. C. Miller, Appl. Phys. Lett. **5**, 17 (1964).

[73] J. Miragliotta, D. K. Wickenden, T. J. Kistenmacher, and W. A. Bryden, J. Opt. Soc. Am. B, **10**, 1447 (1993).

[74] V. Mizrahi and J. E. Sipe, Phys. Rev. B **34**, 3700 (1986).

[75] H. J. Monkhorst and J. D. Pack, Phys. Rev. B **13**, 5188 (1976).

[76] D. J. Moss, E. Ghahramani, J. E. Sipe, and H. M. van Driel, Phys. Rev. B **41**, 1542 (1990).

[77] S. Nakamura, M. Senoh, S. Nagahama, N. Iwasa, T. Yamada, T. Matsushita, H. Kiyoku, and Y. Sugimoto, Appl. Phys. Lett. **68**, 2105 (1996);

[78] S. Nakamura, M. Senoh, S. Nagahama, N. Iwasa, T. Yamada, T. Matsushita, H. Kiyoku, and Y. Sugimoto, Appl. Phys. Lett. **68**, 3269 (1996).

[79] S. Nakamura, M. Senoh, N. Iwasa, S. Nagahama, T. Yamada, and T. Mukai, Jpn. J. Appl. Phys. **34**, L797 (1995).

[80] S. Nakamura, M. Senoh, N. Iwasa, S. Nagahama, T. Yamada, and T. Mukai, Jpn. J. Appl. Phys. **34**, L1332 (1995).

[81] L. Oliveira, Phys. Stat. Sol. (b) **107**, 255 (1981).

[82] J. D. Pack and H. J. Monkhorst, Phys. Rev. B **16**, 1748 (1977).

[83] M. J. Paisley, Z. Sitar, J. B. Posthill, and R. F. Davis, J. Vac. Sci. Technol. A **7**, 701 (1989).

[84] E. D. Palik, *Handbook of optical constants of solids II*, (Academic, Orlando,) 1985.

[85] A. Pasquarello and Antonio Quattropani, Phys. Rev. B **48**, 5090 (1993).

[86] J. P. Perdew and K. Burke, Int. J. Quant. Chem. **57**, 309 (1996).

[87] W. E. Pickett, Computer Physics Reports **9**, 115 (1989).

[88] F. N. H. Robinson, Phys. Lett. **26A**, 435 (1968).

[89] M. Rohlfing, P. Krüger, and J. Pollmann, Phys. Rev. B **48**, 17791 (1993).

[90] A. Rubio, J. L. Corkill, M. L. Cohen, E. L. Shirley, and S. G. Louie, Phys. Rev. B **48**, 11810 (1993).

[91] S. Singh, J. R. Potopowicz, L. G. Van Uitert, and S. H. Wemple, Appl. Phys. Lett. **19**, 53 (1971).

[92] J. J. Sham and M. Schlüter, Phys. Rev. B **32**, 3883 (1985).

[93] Y. R. Shen, *The principles of nonlinear optics,* (New York, Wiley 1984).

[94] S. Singh, *CRC handbook of laser science and technology,* edited by M. J. Weber, (Boca Raton, Fla) 1982.

[95] J. E. Sipe and E. Ghahramani, Phys. Rev. B **48**, 11705 (1993).

[96] Z.Sitar, M. J. Paisley, J. B. Posthill, and R. F. Davis, J. Mater. Sci. Lett. **11**, 261 (1992).

[97] J. C. Slater, *The calculation of molecular orbitals*, (New York, Wiley, 1979).

[98] S. Strite, M. E. Lin, and H. Morkoc, Thin Solid Films **231**, 197 (1993).

[99] M. P. Surh, S. G. Louie, and M. L. Cohen, Phys. Rev. B **43**, 9126 (1991).

[100] M. Teter, Phys. Rev. B **48**, 5031 (1993).

[101] N. Troullier and J. L. Martins, Phys. Rev. B **43**, 1993 (1991).

[102] A. R. Verma and P. Krishna, *Polymorphism and polytypism in crystals*, (Wiley, New York, 1966).

[103] B. Wenzien, P. Käckell, and F. Bechstdet, Phys. Rev. B **52**, 10897 (1995).

[104] E. P. Wigner, Trans. Faraday Soc. **34**, 678 (1938).

[105] A. F. Wright and J. S. Nelson, Phys. Rev. B **50**, 2159 (1994).

[106] Y. N. Xu and W. Y. Ching, Phys. Rev. B **44**, 11048 (1991).

[107] Y. N. Xu and W. Y. Ching, Phys. Rev. B **48**, 4335 (1993).

[108] N. Wiser, Phys. Rev. **129**, 62 (1962).

[109] H. Zhong, Ph.D thesis, Ohio State University (1993).

[110] H. Zhong, Z. H. Levine, D. C. Allan, and J. W. Wilkins, Phys. Rev. B **48**, 1384 (1993).